IEEE Access
Multidisciplinary | Rapid Review | Open Access Journal

Received March 6, 2020, accepted March 13, 2020, date of publication March 16, 2020, date of current version March 30, 2020.

Digital Object Identifier 10.1109/ACCESS.2020.2981177

Generalized MIMO Sequence Impedance Modeling and Stability Analysis of MMC-HVDC With Wind Farm Considering Frequency Couplings

HAOXIANG ZONG[1], (Student Member, IEEE), CHEN ZHANG[2], JING LYU[1,3], (Member, IEEE), XU CAI[1,3], MARTA MOLINAS[2], (Member, IEEE), AND FANGQUAN RAO[1,3]

[1]Wind Power Research Centre, School of Electronic Information and Electrical Engineering, Shanghai Jiao Tong University, Shanghai 200240, China
[2]Department of Engineering Cybernetics, Norwegian University of Science and Technology (NTNU), 7491 Trondheim, Norway
[3]Key Laboratory of Control of Power Transmission and Conversion of Ministry of Education, Shanghai Jiao Tong University, Shanghai 200240, China

Corresponding author: Jing Lyu (lvjing@sjtu.edu.cn)

This work was supported in part by the National Natural Science Foundation of China under Grant 51837007 and Grant 51907125.

ABSTRACT Recently, small-signal stability of the modular multilevel converter (MMC) based high-voltage direct current (HVDC) transmission for wind farm integration has attracted great attentions. The impedance-based frequency-domain method is an effective tool for such studies, in which the accuracy of the impedance model is of significant importance. Currently, the decoupled single-input single-output (SISO) sequence impedance of the MMC-HVDC system with wind farm is commonly used due to the simplicity in stability analysis. However, since both the MMC and wind farm exhibit frequency coupling behaviors, the decoupled SISO sequence impedance model may lead to inaccurate stability conclusion under certain conditions. In order to improve the model accuracy, based on the harmonic state-space (HSS) modeling approach, this paper proposes a generalized multi-input multi-output (MIMO) sequence impedance model of the MMC-wind farm system. The proposed MIMO impedance model can effectively capture the frequency couplings in the interconnected system, based on which the coupling mechanism of multi-frequency components within the MMC is then revealed. To facilitate the interconnection analysis, the model truncation criteria is proposed and validated by comparing the accuracy of the MIMO model with different truncated dimensions. In addition, this paper considers the internal impedance network of the wind farm when developing the aggregated wind farm impedance model for interaction stability analysis. Finally, the proposed MIMO sequence impedance model is applied to accurately predict the instability of the MMC-HVDC connected wind farm system.

INDEX TERMS Wind farm, modular multilevel converter, frequency coupling, sequence impedance, stability.

I. INTRODUCTION

Modular Multilevel Converter (MMC) [1] -based high voltage direct current (HVDC) transmission is the preferred scheme for grid integration of large-scale long-distance offshore wind farms, as shown in Figure 1, thanks to its modularity, scalability, high efficiency, [2], [3], etc. In the last ten years, more than ten MMC-HVDC projects have been commissioned all over the world, especially in China and Germany. However, frequent occurrences of wide-band oscillations in the actual MMC-HVDC systems greatly hinder the project development. Therefore, for practical application, it is very important to accurately predict the small-signal instability of such interconnected system.

To study such small-signal stability problems, both the state space-based [4] and the impedance-based methods

The associate editor coordinating the review of this manuscript and approving it for publication was Zhixiang Zou.

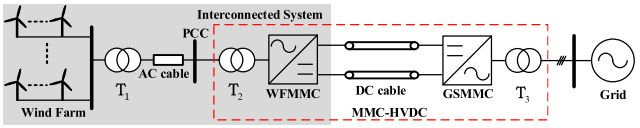

FIGURE 1. Structure diagram of wind farm integration via MMC-HVDC.

can be applied. In this work, the impedance-based method is preferred, since most of the oscillations are caused by port-interactions between source and load subsystem, for which the input-output characteristic is analyzed. The sub-synchronous oscillation phenomenon in a real MMC-HVDC connected with wind farm was first reported in [5], where the impedance-based method was applied to investigate the interaction mechanism. However, the Ref [5] does not consider the effect of the submodule capacitor voltage ripples on the MMC impedance. This flaw is remedied in Ref [6], where the three-phase phase-domain controller in abc stationary frame is adopted. Based on the model of MMC in Ref [6], the stabilization control and the controller parameter optimal design were proposed in [7] and [8] respectively to improve the stability of the interconnected system. The [9] analyzed the stability of a self-synchronization-based wind farm with MMC-HVDC. The low-frequency oscillation around the fundamental frequency in the doubly-fed induction generator (DFIG) based wind farm with MMC-HVDC was studied in [10]. However, most of the interconnected stability analysis were based on the decoupled single-input-single-output (SISO) sequence impedances. The frequency couplings inside the MMC and its influence imposed on the interconnected system have not been studied deeply.

Due to the unique characteristics of the MMC's multi-frequency responses, the accurate characterization of non-negligible frequency couplings is the first key issue for the MMC modeling. Recently, several methods, such as multi-harmonic linearization [11] and harmonic state-space (HSS) [12], [13], have so far been proposed for the MMC impedance modeling. In [12], the HSS method was applied in the MMC impedance modeling considering the internal dynamics effects. And the [11] utilized the multi-harmonic linearization method to include the d-q current loop and phase-lock loop (PLL). However, the above resulting models for analysis are still based on the conventional definition of sequence impedance, which are actually decoupled SISO models focusing on the input and output relationship at the same frequency. In [13], a two-by-two impedance matrix is derived to incorporate the influence of frequency couplings, in which, however, the MMC is used for feeding a linear system that does not exhibit the frequency coupling behavior. For this paper, the MMC is used for integrating the wind farm where the frequency couplings exist in both systems, thus the resulting frequency coupling behavior is worth being clarified. The second key issue is how to capture the dominant frequency couplings and reduce the dimension of the MIMO impedance model for the sake of complex interaction analysis. According to [12], at least the third harmonic needs to be considered to ensure the accuracy of the MMC impedance model. Alternatively, this paper aims at a truncation method by exploiting the property of frequency couplings of the MMC-wind farm system.

The third issue is to improve the accuracy of wind farm aggregation model, rather than adopting the simplified single-machine aggregation model as in the past researches [5]–[10], which is not able to reflect the internal characteristics of the wind farm. The detailed internal electrical network of the wind farm will be considered in this paper when implementing the interaction stability analysis of the MMC-wind farm system. The impedance modeling of the wind turbine is well-established such as Type IV [14] and Type III [15] wind turbine. Nevertheless, careful attention should be paid to the reference frame transformation of individual impedances when formulating the final wind farm impedance. This issue has been well-discussed in [16]–[18] to acquire an accurate impedance aggregation model.

The main contribution of this paper includes: 1) the more accurate and generalized MIMO impedance model of the MMC is proposed, and the frequency couplings within the MMC are clarified not only considering the mirror frequency coupling effect but also the sequence coupling effect; 2) a feasible model truncation criterion is proven, which is sufficient for the interaction stability assessment of the MMC-wind farm interconnected system under balanced three-phase conditions; 3) the impedance network based wind farm aggregated model is adopted to improve the accuracy of the interaction stability analysis.

The rest of the paper is organized as below. In Section II, the generalized MIMO sequence impedance model of the MMC is established using the HSS modeling method. In Section III, the frequency coupling mechanism inside the MMC is illustrated, based on which a reasonable truncated sequence impedance matrix is extracted. Besides, the accuracy of the proposed MIMO impedance models with different truncated dimensions is also compared. In Section IV, a case study on the MMC-HVDC connected wind farm system is carried out to show the effectiveness and accuracy of the derived sequence impedance model considering the frequency couplings. Section V concludes the paper.

II. MIMO SEQUENCE IMPEDANCE MODEL OF THE MMC

Since this paper is mainly focused on the interconnected system with wind farm and wind farm side MMC (WFMMC), the grid-side MMC (GSMMC) shown in Figure 1 can be represented by a dc voltage source and the detailed interconnected system is shown in Figure 2. In this section, the MIMO sequence impedance of the MMC is developed considering multiple harmonics couplings. Compared with [11], the derivation process in this paper is more straightforward and the obtained sequence impedance model not only considers the input/output relationship at the same frequency, but also incorporates other frequency components. Different from the

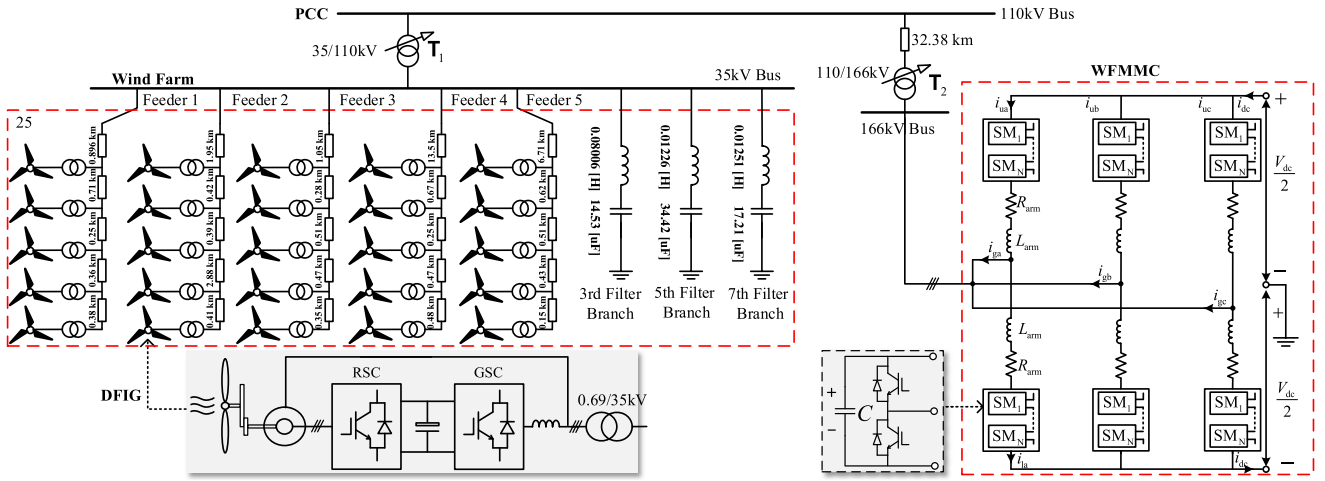

FIGURE 2. Topology of the wind-farm MMC interconnected system.

Ref [6] and Ref [12], the commonly-used double-loop control is also incorporated into the MMC modeling.

A. LINEARIZED THREE-PHASE STATE-SPACE MODEL OF THE MMC

The topology of the MMC is given in Figure 2. The modeling of the main circuit of the MMC in *abc* frame [19] is briefly summarized in Eq. (1).

$$\begin{cases} \dfrac{\mathrm{d}\boldsymbol{i}_{cx}}{\mathrm{d}t} = -\dfrac{R}{L}\boldsymbol{i}_{cx} - \dfrac{\boldsymbol{n}_{ux}}{2L}\boldsymbol{v}_{cux} - \dfrac{\boldsymbol{n}_{lx}}{2L}\boldsymbol{v}_{clx} \\ \dfrac{\mathrm{d}\boldsymbol{v}_{cux}}{\mathrm{d}t} = \dfrac{\boldsymbol{n}_{ux}}{C_{\mathrm{arm}}}\left(\boldsymbol{i}_{cx} + \dfrac{1}{2}\boldsymbol{i}_{gx}\right) \\ \dfrac{\mathrm{d}\boldsymbol{v}_{clx}}{\mathrm{d}t} = \dfrac{\boldsymbol{n}_{lx}}{C_{\mathrm{arm}}}\left(\boldsymbol{i}_{cx} - \dfrac{1}{2}\boldsymbol{i}_{gx}\right) \\ \dfrac{\mathrm{d}\boldsymbol{i}_{gx}}{\mathrm{d}t} = \dfrac{\boldsymbol{n}_{lx}}{L}\boldsymbol{v}_{clx} - \dfrac{\boldsymbol{n}_{ux}}{L}\boldsymbol{v}_{cux} - \dfrac{R}{L}\boldsymbol{i}_{gx} - \dfrac{\boldsymbol{v}_{gx}}{L} \end{cases} \tag{1}$$

where $\boldsymbol{i}_{cx}$, $\boldsymbol{v}_{cux}$, $\boldsymbol{v}_{clx}$, $\boldsymbol{i}_{gx}$, $\boldsymbol{v}_{gx}$ $(x = a, b, c)$ represent the time-periodic circulating current, upper arm voltage, lower arm voltage and ac-side current, respectively. For a nonlinear system in Eq. (1), the linearization needs to be applied to acquire its linear model.

$$\begin{cases} \dfrac{\mathrm{d}\Delta\boldsymbol{i}_{cx}}{\mathrm{d}t} = -\dfrac{R}{L}\Delta\boldsymbol{i}_{cx} - \dfrac{\boldsymbol{n}^{\mathrm{s}}_{ux}}{2L}\Delta\boldsymbol{v}_{cux} - \dfrac{\boldsymbol{n}^{\mathrm{s}}_{lx}}{2L}\Delta\boldsymbol{v}_{clx} - \dfrac{\boldsymbol{v}^{\mathrm{s}}_{cux}}{2L} \\ \quad \Delta\boldsymbol{n}_{ux} - \dfrac{\boldsymbol{v}^{\mathrm{s}}_{clx}}{2L}\Delta\boldsymbol{n}_{lx} \\ \dfrac{\mathrm{d}\Delta\boldsymbol{v}_{cux}}{\mathrm{d}t} = \dfrac{\boldsymbol{n}^{\mathrm{s}}_{ux}}{C_{\mathrm{arm}}}\left(\Delta\boldsymbol{i}_{cx} + \dfrac{1}{2}\Delta\boldsymbol{i}_{gx}\right) + \dfrac{1}{C_{\mathrm{arm}}}\left(\boldsymbol{i}^{\mathrm{s}}_{cx} + \dfrac{1}{2}\boldsymbol{i}^{\mathrm{s}}_{gx}\right) \\ \quad \Delta\boldsymbol{n}_{ux} \\ \dfrac{\mathrm{d}\Delta\boldsymbol{v}_{clx}}{\mathrm{d}t} = \dfrac{\boldsymbol{n}^{\mathrm{s}}_{lx}}{C_{\mathrm{arm}}}\left(\Delta\boldsymbol{i}_{cx} - \dfrac{1}{2}\Delta\boldsymbol{i}_{gx}\right) + \dfrac{1}{C_{\mathrm{arm}}}\left(\boldsymbol{i}^{\mathrm{s}}_{cx} - \dfrac{1}{2}\boldsymbol{i}^{\mathrm{s}}_{gx}\right) \\ \quad \Delta\boldsymbol{n}_{lx} \\ \dfrac{\mathrm{d}\Delta\boldsymbol{i}_{gx}}{\mathrm{d}t} = \dfrac{\boldsymbol{n}^{\mathrm{s}}_{lx}}{L}\Delta\boldsymbol{v}_{clx} - \dfrac{\boldsymbol{n}^{\mathrm{s}}_{ux}}{L}\Delta\boldsymbol{v}_{cux} + \dfrac{\boldsymbol{v}^{\mathrm{s}}_{clx}}{L}\Delta\boldsymbol{n}_{lx} - \dfrac{\boldsymbol{v}^{\mathrm{s}}_{cux}}{L} \\ \quad \Delta\boldsymbol{n}_{ux} - \dfrac{R}{L}\Delta\boldsymbol{i}_{gx} - \dfrac{\Delta\boldsymbol{v}_{gx}}{L} \end{cases} \tag{2}$$

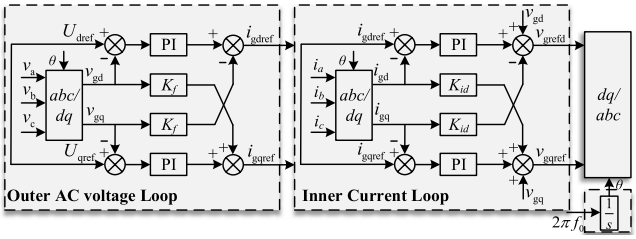

FIGURE 3. Block diagram of the ac voltage control loop of WFMMC.

where the superscript s represents the periodic steady-state value of state variables. Since the WFMMC operates at the ac voltage control mode, only fundamental-frequency component will exist in the modulation indices, whose linearized form is

$$\begin{cases} \Delta\boldsymbol{n}_{ux} = -\dfrac{\Delta\boldsymbol{v}^{\mathrm{ref}}_{gx}}{V_{\mathrm{dc}}} \\ \Delta\boldsymbol{n}_{lx} = \dfrac{\Delta\boldsymbol{v}^{\mathrm{ref}}_{gx}}{V_{\mathrm{dc}}} \end{cases} \tag{3}$$

Now the linearized three-phase state-space model of the MMC main circuit is established, then the next step is to calculate the modulation signal $\Delta\boldsymbol{v}^{\mathrm{ref}}_{gx}$ of the control part. The commonly-used double-loop *d*-*q* control scheme [10] is considered in this paper as shown in Figure 3.

The outer loop can be descripted like

$$\begin{aligned} \boldsymbol{i}^{\mathrm{ref}}_{gdq} &= K_{\mathrm{pv}}\left(\boldsymbol{U}^{\mathrm{ref}}_{dq} - \boldsymbol{v}_{gdq}\right) + K_{\mathrm{iv}}\boldsymbol{x}_{dq1} + K_{\mathrm{f}}\boldsymbol{v}_{gdq} \\ \frac{\mathrm{d}}{\mathrm{d}t}\boldsymbol{x}_{dq1} &= \boldsymbol{U}^{\mathrm{ref}}_{dq} - \boldsymbol{v}_{gdq} \end{aligned} \tag{4}$$

where the $\boldsymbol{x}_{dq1}$ represents the output of the outer loop integrator and the K_{f} is the feedforward gain. The inner loop is like

$$\begin{aligned} \boldsymbol{v}^{\mathrm{ref}}_{gdq} &= K_{\mathrm{pi}}\left(\boldsymbol{i}^{\mathrm{ref}}_{gdq} - \boldsymbol{i}_{gdq}\right) + K_{\mathrm{ii}}\boldsymbol{x}_{dq2} + K_{\mathrm{id}}\boldsymbol{i}_{gqd} \\ \frac{\mathrm{d}}{\mathrm{d}t}\boldsymbol{x}_{dq2} &= \boldsymbol{i}^{\mathrm{ref}}_{gdq} - \boldsymbol{i}_{gdq} \end{aligned} \tag{5}$$

where the $\boldsymbol{x}_{\mathrm{dq2}}$ represents the output of the inner loop integrator and the K_{id} is the decoupling gain equaling to ωL.

To connect with the three-phase model of the MMC main circuit, the state variables of the control part in d-q frame (Eq. (4) & Eq. (5)) need to be transformed into those in abc frame. The transformation of the Eq. (4) is expanded here as an example. The algebraic equation in Eq. (4) is expanded as:

$$\boldsymbol{T}^{\theta}_{dq/abc}\begin{bmatrix} i^{\mathrm{ref}}_{\mathrm{gd}} \\ i^{\mathrm{ref}}_{\mathrm{gq}} \end{bmatrix} = \boldsymbol{T}^{\theta}_{dq/abc}\left(K_{\mathrm{pv}}\left(\begin{bmatrix} U^{\mathrm{ref}}_{\mathrm{d}} \\ U^{\mathrm{ref}}_{\mathrm{q}} \end{bmatrix} - \begin{bmatrix} v_{\mathrm{gd}} \\ v_{\mathrm{gq}} \end{bmatrix}\right) + K_{\mathrm{iv}}\begin{bmatrix} x_{\mathrm{d1}} \\ x_{\mathrm{q1}} \end{bmatrix} + K_{\mathrm{f}}\begin{bmatrix} v_{\mathrm{gd}} \\ v_{\mathrm{gq}} \end{bmatrix}\right) \tag{6}$$

$$\begin{bmatrix} i^{\mathrm{ref}}_{\mathrm{ga}} \\ i^{\mathrm{ref}}_{\mathrm{gb}} \\ i^{\mathrm{ref}}_{\mathrm{gc}} \end{bmatrix} = \boldsymbol{T}^{\theta}_{dq/abc}\left(\boldsymbol{T}^{\theta}_{abc/dq}K_{\mathrm{pv}}\left(\begin{bmatrix} U^{\mathrm{ref}}_{\mathrm{a}} \\ U^{\mathrm{ref}}_{\mathrm{b}} \\ U^{\mathrm{ref}}_{\mathrm{c}} \end{bmatrix} - \begin{bmatrix} v^{\mathrm{ref}}_{\mathrm{a}} \\ v^{\mathrm{ref}}_{\mathrm{b}} \\ v^{\mathrm{ref}}_{\mathrm{c}} \end{bmatrix}\right) + K_{\mathrm{iv}}\begin{bmatrix} x^{\mathrm{ref}}_{1\mathrm{a}} \\ x^{\mathrm{ref}}_{1\mathrm{b}} \\ x^{\mathrm{ref}}_{1\mathrm{c}} \end{bmatrix} + K_{\mathrm{f}}\begin{bmatrix} v^{\mathrm{ref}}_{\mathrm{a}} \\ v^{\mathrm{ref}}_{\mathrm{b}} \\ v^{\mathrm{ref}}_{\mathrm{c}} \end{bmatrix}\right) \tag{7}$$

The differential equation in Eq. (4) is expanded as:

$$\begin{aligned}\frac{\mathrm{d}}{\mathrm{d}t}\begin{bmatrix} x_{1\mathrm{a}} \\ x_{1\mathrm{b}} \\ x_{1\mathrm{c}} \end{bmatrix} &= \frac{\mathrm{d}}{\mathrm{d}t}\left(T^{\theta}_{dq/abc}\begin{bmatrix} x_{\mathrm{d1}} \\ x_{\mathrm{q1}} \end{bmatrix}\right) = \omega_0\frac{\mathrm{d}}{\mathrm{d}\theta}\left(T^{\theta}_{dq/abc}\right)\cdot\begin{bmatrix} x_{\mathrm{d1}} \\ x_{\mathrm{q1}} \end{bmatrix} \\ &\quad + \boldsymbol{T}^{\theta}_{dq/abc}\frac{\mathrm{d}}{\mathrm{d}t}\begin{bmatrix} x_{\mathrm{d1}} \\ x_{\mathrm{q1}} \end{bmatrix} \\ &= \omega_0\frac{\mathrm{d}}{\mathrm{d}\theta}\left(\boldsymbol{T}^{\theta}_{dq/abc}\right)\cdot\boldsymbol{T}^{\theta}_{abc/dq}\begin{bmatrix} x_{\mathrm{a}} \\ x_{\mathrm{b}} \\ x_{\mathrm{c}} \end{bmatrix} \\ &\quad + \boldsymbol{T}^{\theta}_{dq/abc}\left(\boldsymbol{T}^{\theta}_{abc/dq}\begin{bmatrix} U^{\mathrm{ref}}_{\mathrm{a}} \\ U^{\mathrm{ref}}_{\mathrm{b}} \\ U^{\mathrm{ref}}_{\mathrm{c}} \end{bmatrix} - \boldsymbol{T}^{\theta}_{abc/dq}\begin{bmatrix} v^{\mathrm{ref}}_{\mathrm{a}} \\ v^{\mathrm{ref}}_{\mathrm{b}} \\ v^{\mathrm{ref}}_{\mathrm{c}} \end{bmatrix}\right)\end{aligned} \tag{8}$$

The vector form of the Eq. (7) and Eq (8) is given below:

$$\begin{aligned}\boldsymbol{i}^{\mathrm{ref}}_{gx} &= \boldsymbol{T}^{\theta}_{dq/abc}\left(\boldsymbol{T}^{\theta}_{abc/dq}\left(K_{\mathrm{pv}}\left(\boldsymbol{U}^{\mathrm{ref}}_{gx}\right.\right.\right. \\ &\quad \left.\left.\left. -\boldsymbol{v}_{gx}\right) - K_{\mathrm{f}}\boldsymbol{v}_{gx} + K_{\mathrm{iv}}\boldsymbol{x}_{1x}\right)\right)\end{aligned} \tag{9}$$

$$\begin{aligned}\frac{\mathrm{d}\boldsymbol{x}_{1x}}{\mathrm{d}t} &= \omega_0\frac{\mathrm{d}}{\mathrm{d}\theta}\left(\boldsymbol{T}^{\theta}_{abc/dq}\right)\cdot\boldsymbol{T}^{\theta}_{abc/dq}\boldsymbol{x}_{1x} + \boldsymbol{T}^{\theta}_{dq/abc}\cdot\boldsymbol{T}^{\theta}_{abc/dq} \\ &\quad \times\left(\boldsymbol{U}^{\mathrm{ref}}_{gx} - \boldsymbol{v}_{gx}\right)\end{aligned} \tag{10}$$

where the $\boldsymbol{x}_{1x}$ represents the three-phase form of the $\boldsymbol{x}_{\mathrm{dq1}}$. The transformation of the inner loop can be derived similarly, which is like:

$$\begin{aligned}\boldsymbol{v}^{\mathrm{ref}}_{gx} &= \boldsymbol{T}^{\theta}_{dq/abc}\left(\boldsymbol{T}^{\theta}_{abc/dq}\left(K_{\mathrm{pi}}\left(\boldsymbol{i}^{\mathrm{ref}}_{gx} - \boldsymbol{i}_{gx}\right) + K_{\mathrm{ii}}\boldsymbol{x}_{2x}\right)\right. \\ &\quad \left. + \boldsymbol{T}^{\theta}_{abc/qd}K_{\mathrm{id}}\boldsymbol{i}_{gx}\right)\end{aligned} \tag{11}$$

$$\begin{aligned}\frac{\mathrm{d}\boldsymbol{x}_{2x}}{\mathrm{d}t} &= \omega_0\frac{\mathrm{d}}{\mathrm{d}\theta}\left(\boldsymbol{T}^{\theta}_{dq/abc}\right)\boldsymbol{T}^{\theta}_{abc/dq}\boldsymbol{x}_{2x} + \boldsymbol{T}^{\theta}_{dq/abc}\boldsymbol{T}^{\theta}_{abc/dq} \\ &\quad \times\left(\boldsymbol{i}^{\mathrm{ref}}_{gx} - \boldsymbol{i}_{gx}\right)\end{aligned} \tag{12}$$

The park and the inverse park transformation used above is given in Appendix A, including $\boldsymbol{T}^{\theta}_{dq/abc}$, $\boldsymbol{T}^{\theta}_{abc/dq}$ and $\boldsymbol{T}^{\theta}_{abc/qd}$.

The linearized form of the Eq. (9) ∼ Eq. (12) is like

$$\begin{cases}\Delta\boldsymbol{i}^{\mathrm{ref}}_{gx} \\ = \boldsymbol{T}^{\theta}_{dq/abc}\left(\boldsymbol{T}^{\theta}_{abc/dq}\left(-\left(K_{\mathrm{pv}} + K_{\mathrm{f}}\right)\cdot\Delta\boldsymbol{v}_{gx} + K_{\mathrm{iv}}\cdot\Delta\boldsymbol{x}_{1x}\right)\right) \\ \dfrac{\mathrm{d}\Delta\boldsymbol{x}_{1x}}{\mathrm{d}t} = \omega_0\dfrac{\mathrm{d}}{\mathrm{d}\theta}\left(\boldsymbol{T}^{\theta}_{abc/dq}\right)\boldsymbol{T}^{\theta}_{abc/dq} \\ \cdot\Delta\boldsymbol{x}_{1x} - \boldsymbol{T}^{\theta}_{dq/abc}\cdot\boldsymbol{T}^{\theta}_{abc/dq}\Delta\boldsymbol{v}_{gx}\end{cases} \tag{13}$$

$$\begin{cases}\Delta\boldsymbol{v}^{\mathrm{ref}}_{gx} \\ = \boldsymbol{T}^{\theta}_{dq/abc}\left(\boldsymbol{T}^{\theta}_{abc/dq}\left(K_{\mathrm{pi}}\left(\Delta\boldsymbol{i}^{\mathrm{ref}}_{gx} - \Delta\boldsymbol{i}_{gx}\right) + K_{\mathrm{ii}}\Delta\boldsymbol{x}_{2x}\right)\right. \\ \left. + \boldsymbol{T}^{\theta}_{abc/qd}K_{\mathrm{id}}\Delta\boldsymbol{i}_{gx}\right) \\ \dfrac{\mathrm{d}\Delta\boldsymbol{x}_{2x}}{\mathrm{d}t} = \omega_0\dfrac{\mathrm{d}}{\mathrm{d}\theta}\left(\boldsymbol{T}^{\theta}_{abc/dq}\right)\boldsymbol{T}^{\theta}_{abc/dq}\Delta\boldsymbol{x}_{2x} \\ + \boldsymbol{T}^{\theta}_{dq/abc}\boldsymbol{T}^{\theta}_{abc/dq}\left(\Delta\boldsymbol{i}^{\mathrm{ref}}_{gx} - \Delta\boldsymbol{i}_{gx}\right)\end{cases} \tag{14}$$

It is noticed that the multiplication terms originating from the park and inverse park transformation are constant matrices defined as $\boldsymbol{k_1}, \boldsymbol{k_2}$ in Eq. (15) and (16), whose values are listed in Appendix. A.

$$\boldsymbol{k}_1 = \boldsymbol{T}^{\theta}_{dq/abc}\cdot\boldsymbol{T}^{\theta}_{abc/dq} \tag{15}$$

$$\boldsymbol{k}_2 = \boldsymbol{T}^{\theta}_{dq/abc}\boldsymbol{T}^{\theta}_{abc/qd} = -\frac{\mathrm{d}}{\mathrm{d}\theta}\left(\boldsymbol{T}^{\theta}_{abc/dq}\right)\boldsymbol{T}^{\theta}_{abc/dq} \tag{16}$$

Now, by integrating Eq. (13) and (14) into Eq. (2) and (3), the linearized three-phase state-space model of the MMC can be obtained in Eq. (17).

$$\frac{\mathrm{d}}{\mathrm{d}t}\boldsymbol{X}\left(t\right)_{18\times1} = \boldsymbol{A}\left(t\right)_{18\times18}\cdot\boldsymbol{X}\left(t\right)_{18\times1} + \boldsymbol{B}\left(t\right)_{18\times18}\cdot\boldsymbol{U}\left(t\right)_{18\times1} \tag{17}$$

where the $\boldsymbol{X}(t)$ are state vectors including $\Delta\boldsymbol{i}_{cx}$, $\Delta\boldsymbol{v}_{cux}$, $\Delta\boldsymbol{v}_{clx}$, $\Delta\boldsymbol{i}_{gx}$, $\Delta\boldsymbol{v}_{gx}$, $\Delta\boldsymbol{x}_{1x}$, $\Delta\boldsymbol{x}_{2x}$, totally 18 variables. $\boldsymbol{U}(t)$ are input vectors containing $\Delta\boldsymbol{v}_{gx}$. $\boldsymbol{A}(t)$ is the state-space matrix and $\boldsymbol{B}(t)$ is the input-space matrix, whose explicit expressions are given in Appendix E.

B. HARMONIC STATE-SPACE MODEL OF THE MMC

The state-space model of the MMC in Eq. (17) is still time-periodic, which needs to be converted into the harmonic state-space (HSS) model in frequency domain. In HSS, variables are transformed from time domain into the frequency domain, presented by Fourier coefficients as:

$$x\left(t\right) = \sum_{k\in\mathbb{Z}}X_k e^{jk\omega_1 t} \tag{18}$$

By expanding Eq. (17) into the Fourier series, we get

$$\Delta\dot{\boldsymbol{x}}\left(t\right) = \sum\boldsymbol{A}_n e^{jn\omega_1 t}\Delta x + \sum\boldsymbol{B}_n e^{jn\omega_1 t}\Delta\boldsymbol{u} \tag{19}$$

in which $\boldsymbol{A}_{\mathrm{n}}$ and $\boldsymbol{B}_{\mathrm{n}}$ are the Fourier coefficients of $\boldsymbol{A}$(t) and $\boldsymbol{B}$(t) respectively and ω_1 is the fundamental frequency. Taking Laplace transform on Eq (19), we have

$$s\Delta\boldsymbol{x}\left(s\right) = \sum\boldsymbol{A}_n\Delta\boldsymbol{x}\left(s - jn\omega_1\right) + \sum\boldsymbol{B}_n\Delta\boldsymbol{u}\left(s - jn\omega_1\right) \tag{20}$$

The Eq. (20) can be written in matrix form as

$$\boldsymbol{sX} = (\boldsymbol{A} - \boldsymbol{N}) \cdot \boldsymbol{X} + \boldsymbol{B} \cdot \boldsymbol{U} \tag{21}$$

The Equation (21) can be rewritten as (22). It is pointed out that the matrix ($\boldsymbol{A}$-$\boldsymbol{N}_\mathrm{p}$) should be full rank [12].

$$\boldsymbol{X}_p = -\left(\boldsymbol{A} - \boldsymbol{N}_p\right)^{-1} \boldsymbol{B} \cdot \boldsymbol{U}_p \left(\boldsymbol{N}_p = s\boldsymbol{I} + \boldsymbol{N}\right) \tag{22}$$

According to [12], the harmonic order of the HSS is set as three to guarantee the enough accuracy. The $\boldsymbol{X}_\mathrm{p}$ and $\boldsymbol{N}_\mathrm{p}$ are defined in Eq. (23) and Eq. (24).

$$\begin{cases} \boldsymbol{X}_p = \left[\, \boldsymbol{X}_{(\omega_p - 3\omega_1)} \ \cdots \ \boldsymbol{X}_{(\omega_p)} \ \cdots \ \boldsymbol{X}_{(\omega_p + 3\omega_1)} \,\right]^T \\ \boldsymbol{X}_{(\omega_p \pm h\omega_1)} \\ = \left(\left[\, \Delta \boldsymbol{i}_{cx} \ \Delta \boldsymbol{v}_{\mathrm{cux}} \ \Delta \boldsymbol{v}_{\mathrm{clx}} \ \Delta \boldsymbol{i}_{\mathrm{gx}} \ \Delta \boldsymbol{x}_{1x} \ \Delta \boldsymbol{x}_{2x} \,\right]\right)_{1\times 18}^{(\omega_p \pm h\omega_1)} \end{cases} \tag{23}$$

$$\boldsymbol{N}_p = \begin{bmatrix} j\left(\omega_p - 3\omega_1\right)\boldsymbol{I} & & & \\ & \ddots & & \\ & & j\omega_p \boldsymbol{I} & \\ & & & \ddots \\ & & & j\left(\omega_p + 3\omega_1\right)\boldsymbol{I} \end{bmatrix} \tag{24}$$

The Toeplitz matrix of the Fourier coefficients of the system matrix $\boldsymbol{A}$(t) is shown in Eq. (25). The form of the Toeplitz matrix $\boldsymbol{B}$ is the same as the $\boldsymbol{A}$. It is pointed out that there mainly exists dc, fundamental, and double-frequency components in the capacitor voltages and arm currents of the MMC under normal conditions. Therefore, those harmonics above double-frequency can be ignored.

$$\boldsymbol{A}_{126\times 126} = \begin{pmatrix} \boldsymbol{A}_0 & \boldsymbol{A}_{-1} & \boldsymbol{A}_{-2} & & & \\ \boldsymbol{A}_1 & \boldsymbol{A}_0 & \boldsymbol{A}_{-1} & \ddots & & \\ \boldsymbol{A}_2 & \boldsymbol{A}_1 & \ddots & \ddots & \ddots & \\ & \ddots & \ddots & \ddots & \boldsymbol{A}_{-1} & \boldsymbol{A}_{-2} \\ & & \ddots & \boldsymbol{A}_1 & \boldsymbol{A}_0 & \boldsymbol{A}_{-1} \\ & & & \boldsymbol{A}_2 & \boldsymbol{A}_1 & \boldsymbol{A}_0 \end{pmatrix} \tag{25}$$

The perturbation voltage $\boldsymbol{U}_\mathrm{p}$ can be either positive- or negative-sequence. To acquire a $n \times n$ impedance matrix, n perturbations at different frequencies need to be injected. If the perturbation is injected at ω_p, the $\boldsymbol{U}_\mathrm{p}$ is like:

$$\begin{cases} \boldsymbol{U}_p = \left[\, \boldsymbol{U}_{(\omega_p - 3\omega_1)} \ \cdots \ \boldsymbol{U}_{(\omega_p)} \ \cdots \ \boldsymbol{U}_{(\omega_p + 3\omega_1)} \,\right]^T \\ \boldsymbol{U}_{(\omega_p)} = \left[\, \boldsymbol{0}_{3\times 1} \ \boldsymbol{0}_{3\times 1} \ \boldsymbol{0}_{3\times 1} \ \Delta \boldsymbol{v}_{\mathrm{g}x}^{\omega_p} \ \boldsymbol{0}_{3\times 1} \ \boldsymbol{0}_{3\times 1} \,\right] \end{cases} \tag{26}$$

The essence of the impedance calculation is to establish the relationship between the perturbation voltage and the resulting current. The perturbation voltage and the feedback ac current need to be extracted from the $\boldsymbol{X}_\mathrm{p}$ as:

$$\begin{aligned} \boldsymbol{V}_{\mathrm{g}x} &= \left[\, \Delta \boldsymbol{v}_{gx}^{\omega_p - 3\omega_1} \ \cdots \ \Delta \boldsymbol{v}_{gx}^{\omega_p} \ \cdots \ \Delta \boldsymbol{v}_{gx}^{\omega_p + 3\omega_1} \,\right]^T \\ \boldsymbol{I}_{\mathrm{g}x} &= \left[\, \Delta \boldsymbol{i}_{gx}^{\omega_p - 3\omega_1} \ \cdots \ \Delta \boldsymbol{i}_{gx}^{\omega_p} \ \cdots \ \Delta \boldsymbol{i}_{gx}^{\omega_p + 3\omega_1} \,\right]^T \end{aligned} \tag{27}$$

C. DERIVATION OF THE MIMO SEQUENCE IMPEDANCE OF THE MMC

The linear symmetric transformation [20] is applied here to transform state variables in *abc* domain to those in sequence domain. The zero-sequence is omitted because there are no paths for zero-sequence currents. The symmetric transform is extended as:

$$\boldsymbol{E} = diag\left(\ldots, \boldsymbol{e}, \boldsymbol{e}, \boldsymbol{e}, \ldots\right), \quad \boldsymbol{e} = \frac{1}{3}\begin{bmatrix} 1 & e^{j\frac{2\pi}{3}} & e^{-j\frac{2\pi}{3}} \\ 1 & e^{-j\frac{2\pi}{3}} & e^{j\frac{2\pi}{3}} \end{bmatrix} \tag{28}$$

The sequence component of the ac-side voltage $\boldsymbol{U}_\mathrm{gabc}$ and current $\boldsymbol{I}_\mathrm{gabc}$ can be gotten as.

$$\begin{aligned} \boldsymbol{I}_{\mathrm{gpn}} &= \boldsymbol{E} \cdot \boldsymbol{I}_{\mathrm{g}x} = \left[\, \Delta \boldsymbol{i}_{\mathrm{gpn}}^{\omega_p - 3\omega_1} \ \cdots \ \Delta \boldsymbol{i}_{\mathrm{gpn}}^{\omega_p} \ \cdots \ \Delta \boldsymbol{i}_{\mathrm{gpn}}^{\omega_p + 3\omega_1} \,\right]^T \\ \boldsymbol{V}_{\mathrm{gpn}} &= \boldsymbol{E} \cdot \boldsymbol{V}_{\mathrm{g}x} \\ &= \left[\, \Delta \boldsymbol{v}_{\mathrm{gpn}}^{\omega_p - 3\omega_1} \ \cdots \ \Delta \boldsymbol{v}_{\mathrm{gpn}}^{\omega_p} \ \cdots \ \Delta \boldsymbol{v}_{\mathrm{gpn}}^{\omega_p + 3\omega_1} \,\right]^T \end{aligned} \tag{29}$$

Therefore, the MIMO sequence impedance can be derived as:

$$\boldsymbol{Z}_{14\times 14}^{pn} = \boldsymbol{V}_{\mathrm{gpn}} \cdot \left(\boldsymbol{I}_{\mathrm{gpn}}\right)^{-1} \tag{30}$$

III. FREQEUNCY COUPLING ANALYSIS AND TRUNCATION OF THE MMC MIMO SEQUENCE IMPEDANCE

The developed MMC sequence impedance above is of large dimension which is not suitable for numeric stability assessment. In order to derive an appropriate model order for efficient stability analysis, the harmonics coupling inside the MMC especially the frequency couplings should be first analyzed and elucidated. The parameters of the interconnected system are listed in Appendix. B.

A. THE MULTI-FREQUENCY RESPONSE CHARACTERISTICS OF THE MMC

This part will discuss the multi-frequency response characteristics of the LTP system like MMC. The Eq. (22) could be rewritten as:

$$\boldsymbol{X}_p = \underbrace{-\left(\boldsymbol{A} - \boldsymbol{N}_p\right)^{-1} \boldsymbol{B}}_{\mathfrak{R}} \cdot \boldsymbol{U}_p \tag{31}$$

whose matrix form is like:

$$\begin{pmatrix} \vdots \\ \Delta \boldsymbol{x}\left(s_{-1}\right) \\ \Delta \boldsymbol{x}\left(s_0\right) \\ \Delta \boldsymbol{x}\left(s_{+1}\right) \\ \vdots \end{pmatrix} = \begin{pmatrix} \ddots & & & \iddots \\ & \boldsymbol{R}_0\left(s_{-1}\right) & \boldsymbol{R}_{-1}\left(s_0\right) & \boldsymbol{R}_{-2}\left(s_{+1}\right) & \\ & \boldsymbol{R}_1\left(s_{-1}\right) & \boldsymbol{R}_0\left(s_0\right) & \boldsymbol{R}_{-1}\left(s_{+1}\right) & \\ & \boldsymbol{R}_2\left(s_{-1}\right) & \boldsymbol{R}_1\left(s_0\right) & \boldsymbol{R}_0\left(s_{+1}\right) & \\ \iddots & & & & \ddots \end{pmatrix} \cdot \begin{pmatrix} \vdots \\ \Delta \boldsymbol{u}\left(s_{-1}\right) \\ \Delta \boldsymbol{u}\left(s_0\right) \\ \Delta \boldsymbol{u}\left(s_{+1}\right) \\ \vdots \end{pmatrix} \tag{32}$$

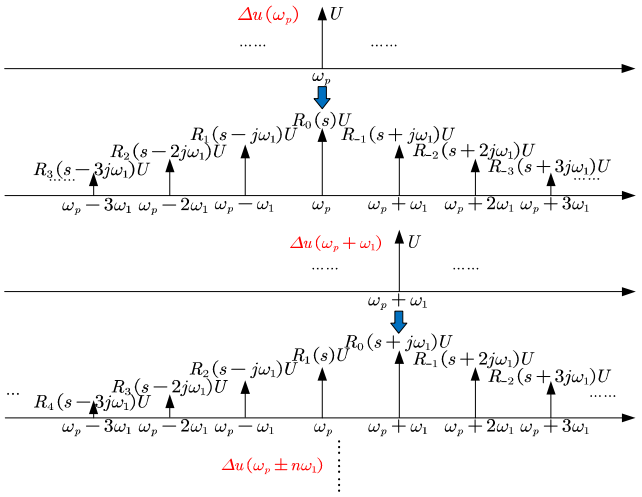

FIGURE 4. Multi-frequency response characteristics of the MMC.

To see the multi-frequency response characteristics represented by the HSS matrix, the $\Delta \boldsymbol{x}(s_0)$ is extracted from Eq. (32) with $s = j\omega$.

$$\Delta \boldsymbol{x}\left(j\omega\right) = \sum_{-h}^{h} \left(\boldsymbol{R}_{-n}\left(j\omega + jn\omega_1\right) \cdot \Delta \boldsymbol{u}\left(j\omega + jn\omega_1\right)\right) \tag{33}$$

Supposing that the input $\Delta \boldsymbol{u}$ only has single frequency ω_{p}, i.e., $\Delta \boldsymbol{u} = \boldsymbol{U}\mathrm{e}^{\mathrm{j}\omega \mathrm{p} t}$, which could be expressed in frequency domain as:

$$\Delta \boldsymbol{u}\left(j\omega\right) = \boldsymbol{U}\delta\left(\omega - \omega_p\right) \tag{34}$$

The corresponding output spectrum is:

$$\Delta \boldsymbol{x}\left(j\omega\right) = \sum_{-h}^{h} \left(\boldsymbol{R}_{-n}\left(j\omega + jn\omega_1\right) \cdot \boldsymbol{U}\delta\left(\omega + n\omega_1 - \omega_p\right)\right) \tag{35}$$

where δ_ω is the Dirac function. It's clear from Eq. (35) that multiple frequencies $\omega_{\mathrm{p}} + n\omega_1$ appear in the output spectrum under single-frequency input which is summarized in Figure.4. Therefore, to acquire a $n \times n$ dimensional matrix, n perturbations need to be injected.

B. ANALYSIS OF THE FREQUENCY COUPLING INSIDE THE MMC

Usually, two main types of couplings exist in the impedance of the converter-based power electronic systems, i.e., frequency coupling and sequence coupling. For the frequency coupling between two different frequencies, it should be defined at the same sequence domain, either positive- or negative-sequence. For the sequence coupling between the positive- and negative-sequence impedances, it should be defined at the same frequency [20].

Thanks to various types of impedance models proposed in recent years, the couplings inside the converters are understood gradually. Divided by the reference frame, there are d-q impedance [21], modified sequence impedance [22], α-β impedance [23] and traditional sequence impedance [24]. Divided by the dimension, there are SISO impedance and MIMO impedance. The above-mentioned impedance models have illustrated the frequency coupling mechanism of the VSC very well, which is mainly originated from the asymmetric d-q control [22] generated by PLL, outer control loop, etc. However, the frequency coupling within the MMC needs further discussions.

As shown in Figure 5 and Figure 6, the injected small-signal perturbation current at 35 Hz will trigger another perturbation current at mirror coupling frequency (65 Hz) either under open-loop control or close-loop control. The frequency couplings exist even under the open-loop control which is totally different from the VSC. In addition to the asymmetric d-q control [22], another important factor producing the frequency coupling within the MMC is the internal double-frequency harmonics, which will interact with the injected frequency making the ac-side exhibiting the frequency coupling characteristics. Therefore, the frequency couplings of the MMC could not be ignored under any control modes as long as the double-frequency harmonics existing. Another noteworthy phenomenon is that, there exist some small harmonics at 1 Hz, 79 Hz, 100 Hz and 121 Hz either under steady-state or small-signal perturbation. These inherent

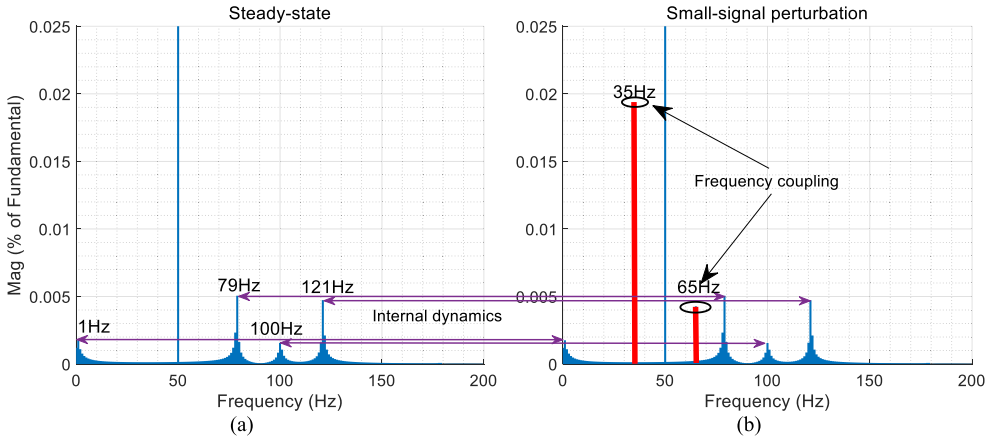

FIGURE 5. Harmonic components of the ac-side current of MMC under open loop control, (a) steady state; (b) small-signal perturbation.

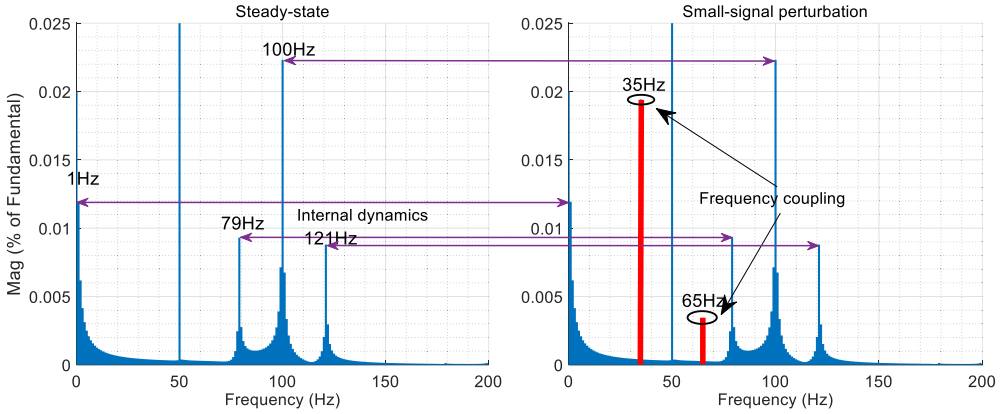

FIGURE 6. Harmonic components of the ac-side current of MMC under closed loop control, (a) steady state; (b) small-signal perturbation.

harmonics are caused by the internal dynamics discussed in [12], that's why the HSS model needs to incorporate the third harmonics.

The distribution of the MIMO sequence impedance derived from the HSS is given in Eq. (36).

$$\begin{bmatrix} \vdots \\ V_p^{+1} \\ V_n^{+1} \\ V_p^{0} \\ V_n^{0} \\ V_p^{-1} \\ V_n^{-1} \\ V_p^{-2} \\ V_n^{-2} \\ \vdots \end{bmatrix} = \begin{bmatrix} \ddots & & & & \ddots & & & \\ & Z_{11}^{0} & 0 & & & Z_{12}^{0} & & \\ & 0 & Z_{22}^{+2} & & & & & \\ & & & Z_{11}^{-1} & 0 & & Z_{12}^{-1} & \\ & & & 0 & Z_{22}^{1} & & & \\ \ddots & & & & & Z_{11}^{-2} & 0 & \ddots \\ & Z_{21}^{0} & & & & 0 & Z_{22}^{0} & \\ & & & & & & Z_{11}^{-3} & 0 \\ & & & Z_{21}^{-1} & & & 0 & Z_{22}^{-1} \\ & & & & \ddots & & & \ddots \end{bmatrix} \times \begin{bmatrix} \vdots \\ I_p^{+1} \\ I_n^{+1} \\ I_p^{0} \\ I_n^{0} \\ I_p^{-1} \\ I_n^{-1} \\ I_p^{-2} \\ I_n^{-2} \\ \vdots \end{bmatrix} \tag{36}$$

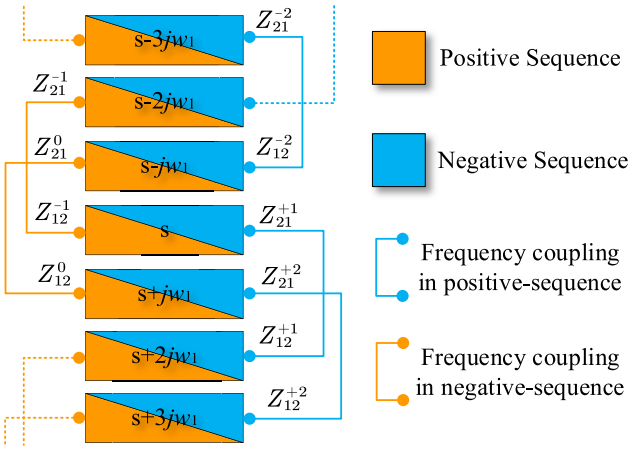

FIGURE 7. Modified distribution of the frequency coupling in positive- and negative-sequence impedances.

According to Ref [25] and [26], when extending the frequency coupling of MIMO impedance matrix, the symmetrical transformation needs to be modified to avoid the frequency coupling happening between sequences. The modified coupling propagation path in positive/negative sequence is given in Figure 7. The arrows represent the coupling between two frequencies. The frequencies in orange color belong to the positive sequence, while the frequencies in blue color belong to the negative sequence. The dotted line means that the frequency coupling will not appear in this truncated frequency range. Taking one pair of the coupled frequency $(s + j\omega_1, s - j\omega_1)$ for example, the frequency coupling appears in the positive-sequence, while it doesn't show up in the negative-sequence. But the frequency couplings in the negative-sequence appears in the third harmonic $(s + 3j\omega_1)$, and the positive-sequence will not exhibit the frequency couplings this time. Therefore, for any given two coupled frequencies, there will only exist one pair of frequency couplings either in positive- or negative-sequence. And the frequency coupling will appear alternately in positive- and negative-sequence impedances.

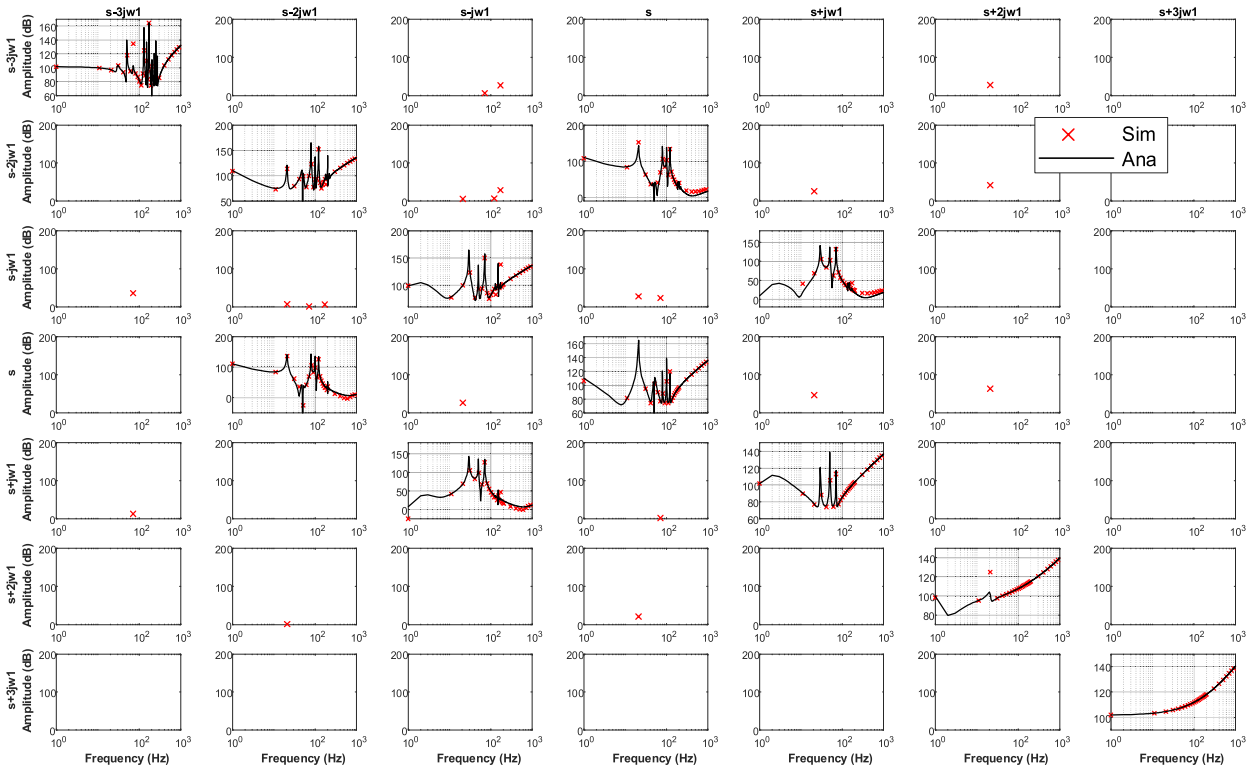

FIGURE 8. Positive-sequence impedance of the MMC (amplitudes).

The positive- and negative- sequence is split as:

$$\begin{bmatrix} V_p^{+3} \\ V_p^{+2} \\ V_p^{+1} \\ V_p^{0} \\ V_p^{-1} \\ V_p^{-2} \\ V_p^{-3} \end{bmatrix} = \begin{bmatrix} Z_{22}^{+4} & & & & & & \\ & Z_{22}^{+3} & & & & & \\ & & Z_{11}^{0} & Z_{12}^{0} & & & \\ & & & Z_{11}^{-1} & Z_{12}^{-1} & & \\ & & Z_{21}^{0} & Z_{22}^{0} & & & \\ & & & Z_{21}^{-1} & Z_{22}^{-1} & & \\ & & & & & & Z_{11}^{-4} \end{bmatrix} \times \begin{bmatrix} I_p^{+3} \\ I_p^{+2} \\ I_p^{+1} \\ I_p^{0} \\ I_p^{-1} \\ I_p^{-2} \\ I_p^{-3} \end{bmatrix} \tag{37}$$

$$\begin{bmatrix} V_n^{+3} \\ V_n^{+2} \\ V_n^{+1} \\ V_n^{0} \\ V_n^{-1} \\ V_n^{-2} \\ V_n^{-3} \end{bmatrix} = \begin{bmatrix} Z_{11}^{+2} & & Z_{12}^{+2} & & & & \\ & Z_{11}^{+1} & & Z_{12}^{+1} & & & \\ Z_{21}^{+2} & & Z_{22}^{+3} & & & & \\ & Z_{21}^{+1} & & Z_{22}^{1} & & & \\ & & & & Z_{11}^{-2} & & Z_{12}^{-2} \\ & & & & & Z_{11}^{-3} & \\ & & & & Z_{21}^{-2} & & Z_{22}^{-2} \end{bmatrix} \times \begin{bmatrix} I_n^{+3} \\ I_n^{+2} \\ I_n^{+1} \\ I_n^{0} \\ I_n^{-1} \\ I_n^{-2} \\ I_n^{-3} \end{bmatrix} \tag{38}$$

The frequency scanning results are given to verify the correctness of the extracted impedance model in Eq. (37) and Eq. (38). As shown in Figure 8, amplitudes of the analytical positive sequence impedance fit well with the results of the frequency scanning. It can be observed that there exist frequency couplings in two set of frequencies: $s + j\omega_1$ and $s - j\omega_1$; $s + 2j\omega_1$ and s. Correspondingly, the negative sequence impedance and its frequency scanning results are given in Figure 9, which also shows a good conformity. Similarly, there exist frequency couplings in three set of frequencies: $s - j\omega_1$ and the $s - 3j\omega_1$, s and $s + 2j\omega_1$, $s + j\omega_1$ and $s + 3j\omega_1$. Unlike the VSC-based wind farm, the off-diagonal terms of the frequency coupling in MMC will decline rapidly in the medium- and high-frequency range, where the frequency couplings in MMC can be ignored.

Therefore, the frequency coupling depicts the coupling at two different frequencies but in the same sequence. The sequence coupling depicts the coupling between positive- and negative-sequence but at the same frequency. In three-phase balanced system, only the frequency coupling needs to be taken into account. And for the MMC, the frequency couplings cannot be ignored, which is the foundation of the model truncation in the following part.

C. TRUNCATION OF THE MMC MIMO SEQUENCE IMPEDANCE MODEL

Actually, the modified sequence impedance [22] reflects the frequency coupling very well. In this section, it's found that the derived MIMO sequence impedance matrix will exhibit

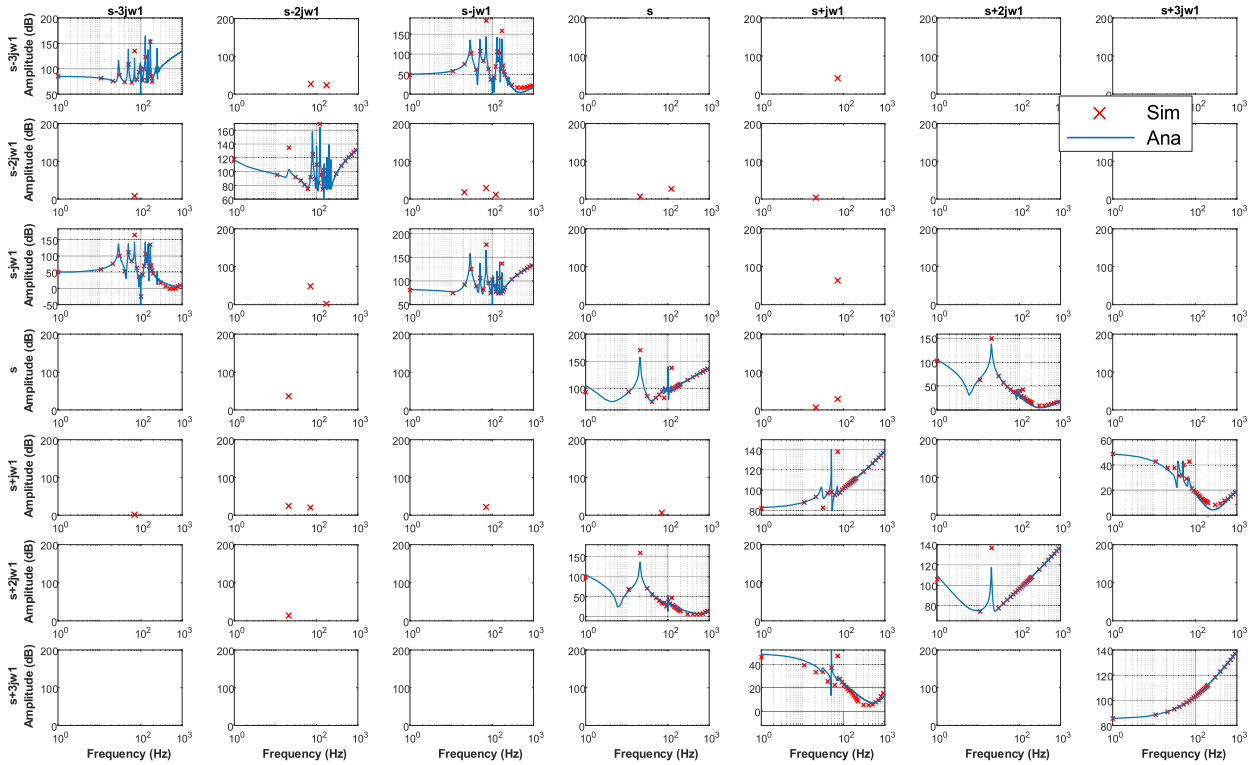

FIGURE 9. Negative-sequence impedance of the MMC (amplitudes).

a more compact distribution in modified sequence domain, which is very helpful for estimating the truncation criteria. Therefore, the MIMO sequence impedance (*p*/*n*) matrix is transformed into the MIMO modified sequence impedance (*Mp*/*Mn*) matrix by using the relationship as:

$$\begin{bmatrix} V_p \\ V_n \end{bmatrix} = \underbrace{\begin{bmatrix} e^{-j\omega_1 t} & 0 \\ 0 & e^{j\omega_1 t} \end{bmatrix}}_{\boldsymbol{P}} \cdot \begin{bmatrix} V_{Mp} \\ V_{Mn} \end{bmatrix} \tag{39}$$

Therefore, the modified sequence impedance could be obtained as:

$$\boldsymbol{Z}_{Mpn} = \boldsymbol{P}_h^{-1} \boldsymbol{Z}_{pn} \boldsymbol{P}_h \tag{40}$$

where the Toeplitz matrix of the $\boldsymbol{P}_h$ is like:

$$\boldsymbol{P}_h = \begin{bmatrix} \ddots & & & & & & & \\ & 0 & 0 & & & & & \\ \ddots & 0 & 1 & & & & & \\ & & & 1 & 0 & & & \ddots \\ & & & 0 & 0 & & & \\ & & & & & 0 & 0 & \\ & & & & & 0 & 1 & \\ & & & & & & & \ddots \end{bmatrix} \tag{41}$$

By integrating Eq. (36) into the Eq. (40), the MIMO modified sequence impedance could be obtained as:

$$\begin{bmatrix} \vdots \\ V_{Mp}^{+1} \\ V_{Mn}^{+1} \\ V_{Mp}^{0} \\ V_{Mn}^{0} \\ V_{Mp}^{-1} \\ V_{Mn}^{-1} \\ \vdots \end{bmatrix} = \begin{bmatrix} \ddots & & & & & & & \\ & Z_{11}^{+1} & Z_{12}^{+1} & & & & & \\ & Z_{21}^{+1} & Z_{22}^{+1} & & & & & \\ & & & Z_{11}^{0} & Z_{12}^{0} & & & \\ & & & Z_{21}^{0} & Z_{22}^{0} & & & \\ & & & & & Z_{11}^{-1} & Z_{12}^{-1} & \\ & & & & & Z_{21}^{-1} & Z_{22}^{-1} & \\ & & & & & & & \ddots \end{bmatrix} \begin{bmatrix} \vdots \\ I_{Mp}^{+1} \\ I_{Mn}^{+1} \\ I_{Mp}^{0} \\ I_{Mn}^{0} \\ I_{Mp}^{-1} \\ I_{Mn}^{-1} \\ \vdots \end{bmatrix} \tag{42}$$

It can be observed from Eq. (42) that under the fundamental frequency rotating frame, the frequency coupling could be rearranged in a more compact form, i.e., diagonal block matrix without decentralized couplings. Therefore,

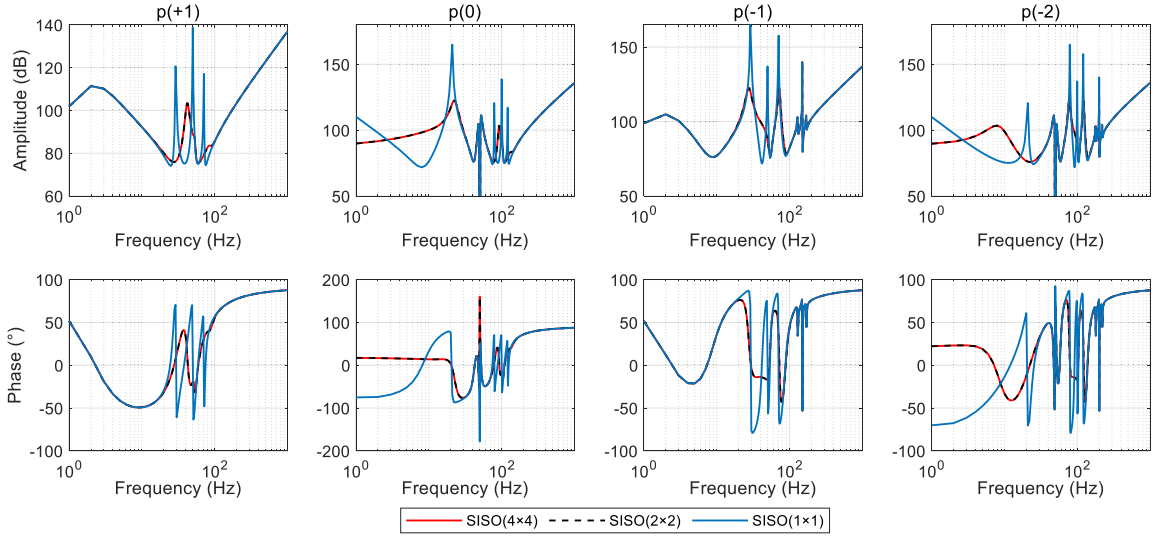

FIGURE 10. Accuracy comparison of the truncated models with different dimensions.

one two-by-two impedance matrix could include all essential information of Eq. (42) or Eq. (36) since the other entries can be gotten by shifting s to s_n ($n = 1; -1; 2; -2; \ldots$). In particular, if s is shifted to s_{-1}, the same model as the one proposed in [22] could be obtained, which has been recognized as a modified sequence impedance in the stationary frame.

$$\begin{bmatrix} V_p(0) \\ V_n(-2) \end{bmatrix} = \begin{bmatrix} Z_{11}^0(s-j\omega_1) & Z_{12}^0(s-j\omega_1) \\ Z_{21}^0(s-j\omega_1) & Z_{22}^0(s-j\omega_1) \end{bmatrix} \begin{bmatrix} I_p(0) \\ I_n(-2) \end{bmatrix} \tag{43}$$

Thus, one two-by-two impedance matrix containing a pair of frequency coupling is enough for stability analysis. The information of the seven-by-seven impedance matrix is duplicated in stability judgement, because it's just the frequency shift of one two-by-two impedance matrix. This conclusion is only valid when MMC operates under three-phase balanced condition. If the MMC went into three-phase unbalanced condition, the order of the MIMO model needs to be raised to incorporate the sequence coupling.

D. ACCURACY COMPARISON OF THE TRUNCATED MODELS WITH DIFFERENT DIMENSIONS

To make the model truncation more persuasive, the accuracy of the model with different dimensions are compared by transforming them into the SISO impedance model (a method introduced in Ref [27]). Here, the four-by-four, two-by-two and one-by-one positive-sequence impedances are compared, whose expressions are like:

$$\begin{bmatrix} V_p^{+1} \\ V_p^0 \\ V_p^{-1} \\ V_p^{-2} \end{bmatrix} = \begin{bmatrix} Z_{11}^0 & & Z_{12}^0 & \\ & Z_{11}^{-1} & & Z_{12}^{-1} \\ Z_{21}^0 & & Z_{22}^0 & \\ & Z_{21}^{-1} & & Z_{22}^{-1} \end{bmatrix}_{4\times4} \begin{bmatrix} I_p^{+1} \\ I_p^0 \\ I_p^{-1} \\ I_p^{-2} \end{bmatrix} \tag{44}$$

$$\begin{bmatrix} V_p^{+1} \\ V_p^{-1} \end{bmatrix} = \begin{bmatrix} Z_{11}^0 & Z_{12}^0 \\ Z_{21}^0 & Z_{22}^0 \end{bmatrix}_{2\times2} \begin{bmatrix} I_p^{+1} \\ I_p^{-1} \end{bmatrix} \tag{45}$$

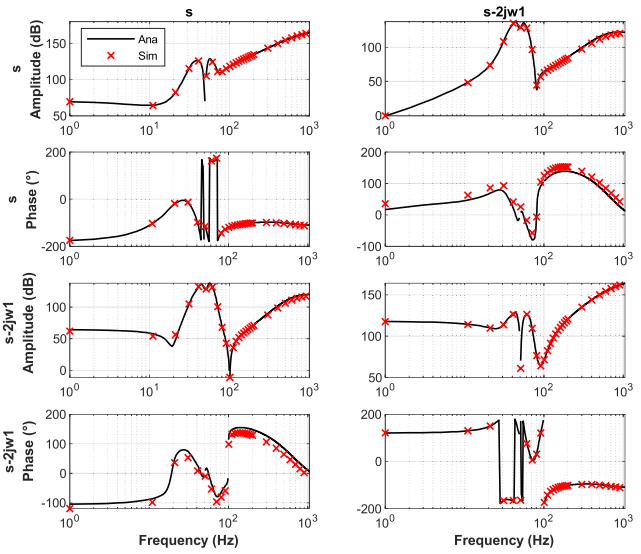

FIGURE 11. Impedance validation of the ZWF p.

$$V_p^{+1} = \left[Z_{11}^0\right]_{1\times1} I_p^{+1}, \quad V_p^{-1} = \left[Z_{22}^0\right]_{1\times1} I_p^{-1} \tag{46}$$

The above three truncated models are compared in Figure 10 via the SISO equivalent impedances [27]. It can be observed that the truncated two-by-two sequence impedance in Eq. (45) could guarantee the sufficient accuracy, which is rewritten as

$$\mathbf{Z}_{\mathrm{P}}^{\mathrm{MMC}} = \begin{bmatrix} Z_{\mathrm{P\_11}}^{\mathrm{MMC}} & Z_{\mathrm{P\_12}}^{\mathrm{MMC}} \\ Z_{\mathrm{P\_21}}^{\mathrm{MMC}} & Z_{\mathrm{P\_22}}^{\mathrm{MMC}} \end{bmatrix} \tag{47}$$

where the subscript P denotes the positive-sequence. The phase verification of one pair of coupled frequencies in positive and negative sequence are listed in Appendix C. The decoupled sequence impedance adopted in the past

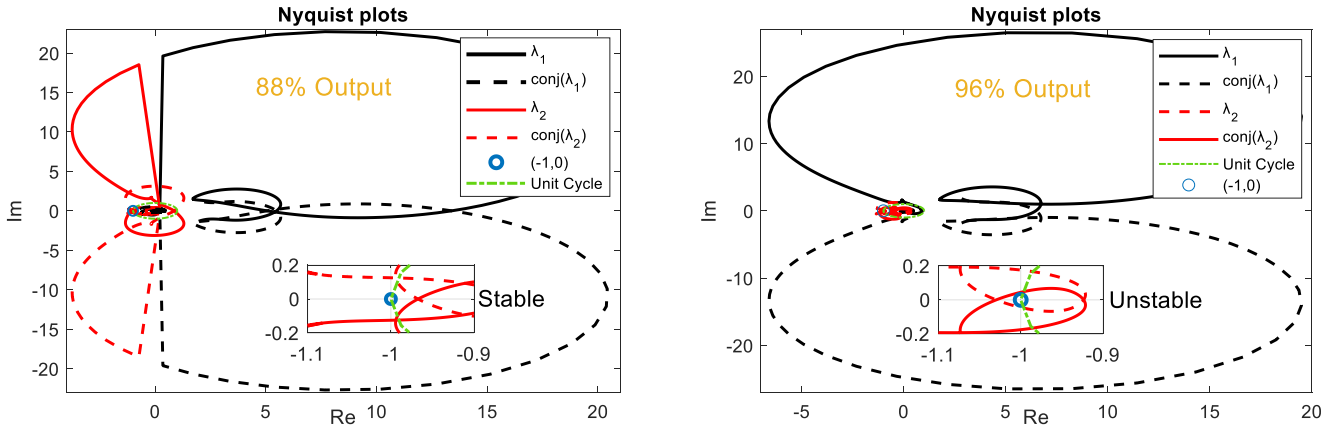

FIGURE 12. Stability analysis considering frequency couplings.

research [5]–[9] ignoring the off-diagonal components is like:

$$\overline{\boldsymbol{Z}_{\mathrm{P}}^{\mathrm{MMC}}}=\begin{bmatrix} Z_{\mathrm{P\_11}}^{\mathrm{MMC}} & 0 \\ 0 & Z_{\mathrm{P\_22}}^{\mathrm{MMC}} \end{bmatrix} \tag{48}$$

IV. STABILITY ANALYSIS OF THE INTERCONNECTED SYSTEM

In this section, the truncated two-by-two sequence impedance of the MMC will be used for stability analysis of the interconnected system. Also, the impedance network-based wind farm aggregation model is also validated.

A. IMPEDANCE VALIDATION OF THE WIND FARM

The impedance network-based wind farm model is adopted in this paper. The accuracy of the model is guaranteed by considering the detailed doubly-fed induction generator-based wind turbine model [14], collection network model, transformers and filter branches. The topology of the wind farm has been given in Figure 2, which contains twenty-five DFIG-based wind turbines, 0.69/35kV transformers and three filter branches. The positive-sequence impedance of the wind farm considering frequency couplings is derived in Appendix D. To match with the truncated MMC positive-sequence impedance, one pair of coupled frequencies is considered which is like

$$\begin{bmatrix} V_{\mathrm{p}}(s) \\ V_{\mathrm{p}}(s-2j\omega_1) \end{bmatrix}=\boldsymbol{Z}_{\mathrm{P}}^{\mathrm{WF}}(s)\cdot\begin{bmatrix} I_{\mathrm{p}}(s) \\ I_{\mathrm{p}}(s-2j\omega_1) \end{bmatrix} \tag{49}$$

where

$$\boldsymbol{Z}_{\mathrm{P}}^{\mathrm{WF}}(s)=\begin{bmatrix} Z_{\mathrm{P\_11}}^{\mathrm{WF}} & Z_{\mathrm{P\_12}}^{\mathrm{WF}} \\ Z_{\mathrm{P\_21}}^{\mathrm{WF}} & Z_{\mathrm{P\_22}}^{\mathrm{WF}} \end{bmatrix} \tag{50}$$

The impedance validation of the positive-sequence impedance of the wind farm is given in Figure 11. It can be seen that both the amplitude and phase of the analytical model fit well with the frequency scanning results. The decoupled

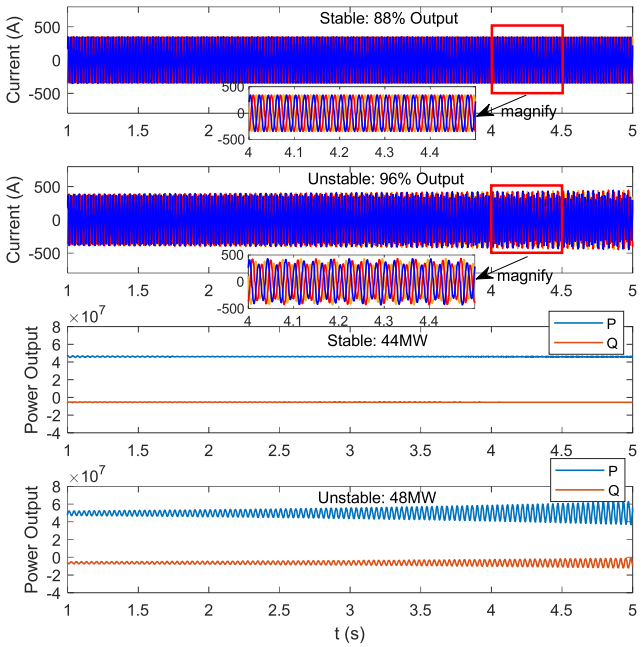

FIGURE 13. Time domain verifications.

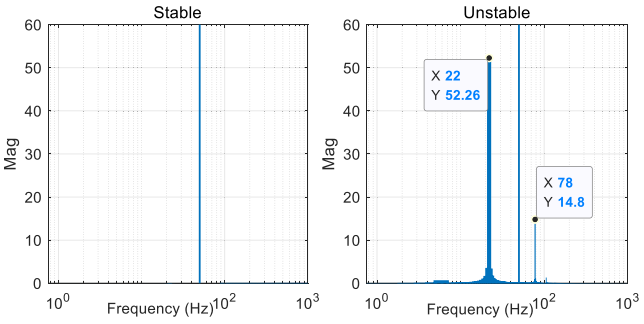

FIGURE 14. FFT analysis of the PCC current.

wind farm sequence impedance is like:

$$\overline{\boldsymbol{Z}_{\mathrm{P}}^{\mathrm{WF}}(s)}=\begin{bmatrix} Z_{\mathrm{P\_11}}^{\mathrm{WF}} & 0 \\ 0 & Z_{\mathrm{P\_22}}^{\mathrm{WF}} \end{bmatrix} \tag{51}$$

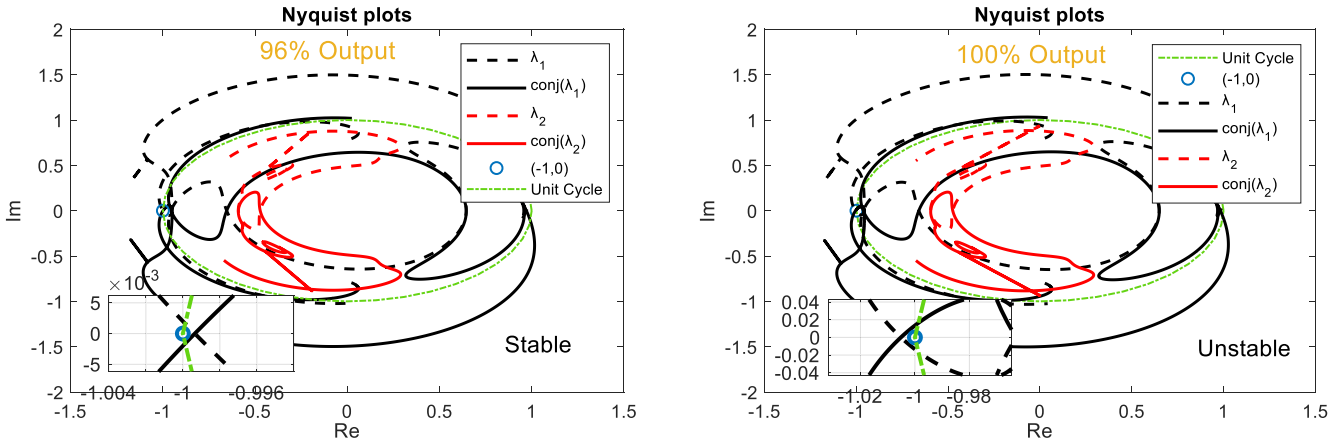

FIGURE 15. Stability analysis without considering frequency couplings.

B. STABILITY ANALYSIS CONSIDERING FREQUENCY COUPLINGS

Actually, the MMC-HVDC connected wind farm is a type 'Z+Y' interconnected system as stated in [28]. According to [28], there will not exist right-half-plane (RHP) poles when the subsystem is stable in stand-alone mode. If the interconnected system can operate normally, the wind farm and MMC-HVDC system will work stably when connected to the ideal voltage or current source in stand-alone mode. Based on this, the effects of the RHP can be excluded. The impedance ratio considering frequency couplings is like

$$\boldsymbol{L}_1 = \boldsymbol{Z}_{\mathrm{p}}^{\mathrm{MMC}}(s) \cdot inv\left(\boldsymbol{Z}_{\mathrm{p}}^{\mathrm{WF}}(s)\right) \tag{52}$$

Because $\boldsymbol{L}_1$ does not contain any right RHP pole, the closed-loop system is stable if and only if the eigen-loci of $\boldsymbol{L}_1$ does not encircle the critical point $(-1, 0j)$. The Nyquist plots are shown in Figure 12. When the output active power of the wind farm approaches 88% of the rated power, the stability margin is small and close to the critical state. When two more wind turbines are put into service (96% of the rated power), the eigen-loci of the $\boldsymbol{L}_1$ encircles the $(-1,0j)$. The theoretical analysis is verified by the time-domain simulations and FFT analysis, as shown in Figure 13 and Figure 14. Under the stable state, the PCC current mainly consists of the fundamental component. Under the unstable state, the oscillation appears at 22 Hz and the coupled term happens at 78 Hz. Therefore, the accuracy of the sequence impedance model considering the frequency couplings has been verified.

C. STABILITY ANALYSIS IGNORING FREQUENCY COUPLINGS

The stability judgement of the same interconnected system based on the decoupled sequence impedance model [5]–[10] is also given in this part. The impedance ratio $\boldsymbol{L}_2$ without considering frequency couplings is like

$$\boldsymbol{L}_2 = \overline{\boldsymbol{Z}_{\mathrm{P}}^{\mathrm{MMC}}(s)} \cdot inv(\overline{\boldsymbol{Z}_{\mathrm{p}}^{\mathrm{WF}}}) \tag{53}$$

As shown in Figure 15, the critical state is indicated when the wind farm output power reaches 96% of the rated power, which is contradictable with the time-domain somulation results in Figure 13. And when the wind farm output power reaches 100% of the rated power, the unstable state is predicted by the conventional stability judgement. Therefore, for the studied system, an optimistic stabilty result is given by the conventional stability judgement without considering the frequency couplings. Worth mentioning that there exist many other cases where the SISO model fails in the stability assessement, this points to the necessity of using a more detailed model for analysis.

V. CONCLUSION

This paper proposes a generalized MIMO sequence impedance model of the MMC, aiming at accurately predicting instabilities of the interconnected wind farm-MMC system. The established MIMO sequence impedance model of the MMC is verified by the frequency scanning. Based on this modeling process, a better understanding of the frequency couplings inside the MMC is achieved. And this knowledge is useful for model truncation since the distribution of frequency couplings is closely related to the model dimension. By comparing the accuracy of the truncated impedance models with different dimensions, the MMC impedance model including one pair of coupled frequency components is proven to be sufficient for the stability analysis under balanced three-phase systems. Finally, the accuracy of the proposed impedance models has been confirmed by both the frequency-domain analysis and time-domain simulations of the MMC-HVDC connected wind farm system. In addition, it is noted that the proposed MMC MIMO impedance model can also be applied for the stability analysis under unbalanced three-phase systems, which will be further discussed in the future work.

APPENDIX

A. SYMBOLS DEFINITION

The park transformation is given in Eq. (A1). The inverse park transformation is given in Eq. (A2). The park transformation when q axis leads d axis is given in Eq. (A3). The constant

TABLE 1. Parameters of the wind farm.

Items	Value	Items	Value
Rated power	2MW	Stator resistance	0.00672pu
Rated voltage	690V	Stator inductance	0.0985pu
Nominal Frequency	50Hz	Rotor resistance	0.00504pu
Mutual inductance	4.316pu	Rotor inductance	0.0996pu
DC link capacitor	10mF	35kV-bus resistance	0.18Ω/km
DC link voltage	1.1kV	35kV-bus inductance	1.2mH/km
Number of DFIG	25	110kV-bus resistance	0.1Ω/km
Filter inductance	0.38mH	110kV-bus inductance	0.5mH/km

TABLE 2. Parameters of the MMC.

Items	Value	Items	Value
Rated power	50MW	Rated voltage	166kV
Nominal Frequency	50Hz	Arm resistance	1Ω
Arm inductance	0.36H	SM number per arm	20
SM capacitance	0.14mF	DC link rated voltage	320kV

$\boldsymbol{k}_1$ and $\boldsymbol{k}_2$ are defined in Eq. (A4).

$$\boldsymbol{T}^{\theta}_{abc/dq} = \frac{2}{3}\cdot\begin{bmatrix} \cos\theta & \cos\left(\theta-\frac{2}{3}\pi\right) & \cos\left(\theta+\frac{2}{3}\pi\right) \\ -\sin\theta & -\sin\left(\theta-\frac{2}{3}\pi\right) & -\sin\left(\theta+\frac{2}{3}\pi\right) \end{bmatrix} \tag{A1}$$

$$\boldsymbol{T}^{\theta}_{dq/abc} = \begin{bmatrix} \cos\theta & \cos\left(\theta-\frac{2}{3}\pi\right) & \cos\left(\theta+\frac{2}{3}\pi\right) \\ -\sin\theta & -\sin\left(\theta-\frac{2}{3}\pi\right) & -\sin\left(\theta+\frac{2}{3}\pi\right) \end{bmatrix}^{T} \tag{A2}$$

$$\boldsymbol{T}^{\theta}_{abc/qd} = \frac{2}{3}\cdot\begin{bmatrix} \sin\theta & \sin\left(\theta-\frac{2}{3}\pi\right) & \sin\left(\theta+\frac{2}{3}\pi\right) \\ \cos\theta & \cos\left(\theta-\frac{2}{3}\pi\right) & \cos\left(\theta+\frac{2}{3}\pi\right) \end{bmatrix} \tag{A3}$$

$$\boldsymbol{k}_1 = \frac{2}{3}\cdot\begin{bmatrix} 1 & -\frac{1}{2} & -\frac{1}{2} \\ -\frac{1}{2} & 1 & -\frac{1}{2} \\ -\frac{1}{2} & -\frac{1}{2} & 1 \end{bmatrix}$$

$$\boldsymbol{k}_2 = \frac{2}{3}\cdot\begin{bmatrix} 0 & -\frac{\sqrt{3}}{2} & \frac{\sqrt{3}}{2} \\ \frac{\sqrt{3}}{2} & 0 & -\frac{\sqrt{3}}{2} \\ -\frac{\sqrt{3}}{2} & \frac{\sqrt{3}}{2} & 0 \end{bmatrix} \tag{A4}$$

B. SYSTEM PARAMETERS

The parameters of the wind farm are listed in Table 1 and the parameters of the MMC station is given in Table 2.

C. SUPPLEMENTARY VALIDATION

The phase verification of the positive-sequence impedance is given in Figure 16, taking one pair of coupled frequencies $(s,\ s-2j\omega_1)$ for example. The phase verification of the negative-sequence impedance is given in Figure 17, taking one pair of coupled frequencies $(s+2j\omega_1,\ s)$ for example.

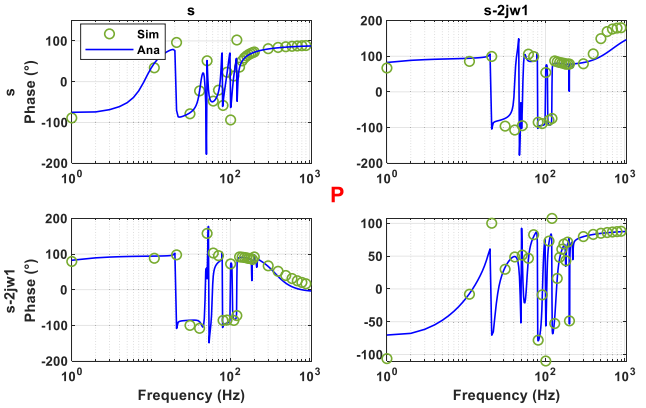

FIGURE 16. Impedance validation of the MMC negative- sequence impedance (Phase).

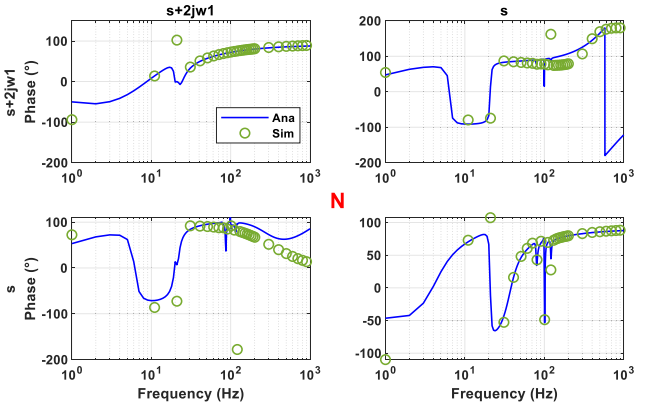

FIGURE 17. Impedance validation of the MMC positive-sequence impedance (Phase).

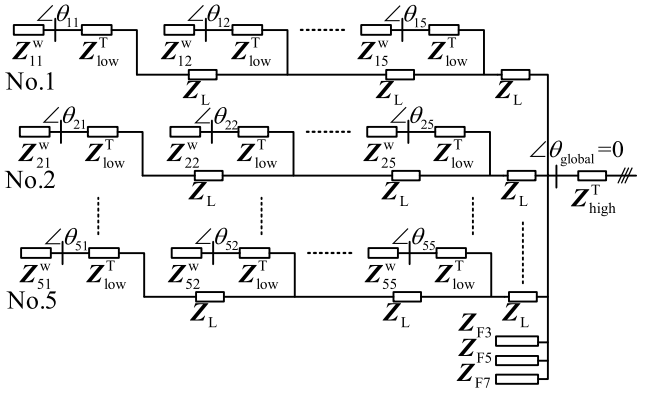

FIGURE 18. Impedance network of the DFIG-based wind farm.

D. IMPEDANC NETWORK-BASED MODELING OF THE WIND FARM

Firstly, the detailed impedance model [16] of the DFIG-based wind turbine is adopted, which considers the dynamics of

the induction generator, rotor-side converter (RSC), grid-side converter (GSC) and dc-link. The whole impedance of the DFIG-based wind turbine contains three parts, i.e., GSC, RSC and equivalent dc-side, which is expressed as

$$\boldsymbol{Z}_{\mathrm{dq}}^{\mathrm{W}} = \boldsymbol{Z}_{\mathrm{dq}}^{\mathrm{gsc}} + \boldsymbol{Z}_{\mathrm{dq}}^{\mathrm{rsc}} + \boldsymbol{Z}_{\mathrm{dq}}^{\mathrm{dc}} \tag{D1}$$

The next step is to establish the impedance network of the wind farm, which shows higher accuracy in stability analysis [16]. The basic idea is to integrate the impedances of the wind turbines, transformers and cables into a circuit network as shown in Figure 18. Since the impedances of the wind turbines are modeled locally, they need to be reoriented to the global reference frame defined at the point of common coupling (PCC). Taking the wind turbine located in the first row and first column for example, a rotation matrix is applied according to the deviation angle of the local voltage, which is like Eq. (D2) and Eq. (D3).

$$\boldsymbol{Z}_{11}^{\mathrm{W}} = \boldsymbol{T}_{\mathrm{dq}}^{11} \boldsymbol{Z}_{\mathrm{dq}}^{\mathrm{W}} \left(\boldsymbol{T}_{\mathrm{dq}}^{11}\right)^{-1} \tag{D2}$$

$$\boldsymbol{T}_{\mathrm{dq}}^{11} = \begin{bmatrix} \cos\theta_{11} & \sin\theta_{11} \\ -\sin\theta_{11} & \cos\theta_{11} \end{bmatrix} \tag{D3}$$

After unifying the *d-q* frame of all wind turbines, the circuit operation could be applied to simplify the impedance network. For example, the accurate output impedance of the feeder 1 of the wind farm is like

$$\begin{cases} \boldsymbol{Z}_{\mathrm{W\_1}}^{1} = \left((\boldsymbol{Z}_{11}^{\mathrm{W}} + \boldsymbol{Z}_{1\mathrm{ow}}^{\mathrm{T}} + \boldsymbol{Z}_{\mathrm{L}})^{-1} + (\boldsymbol{Z}_{12}^{\mathrm{W}} + \boldsymbol{Z}_{1\mathrm{ow}}^{\mathrm{T}})^{-1} \right)^{-1} \\ \vdots \\ \boldsymbol{Z}_{\mathrm{W\_4}}^{1} = \left((\boldsymbol{Z}_{\mathrm{W\_3}}^{1} + \boldsymbol{Z}_{\mathrm{L}})^{-1} + (\boldsymbol{Z}_{15}^{\mathrm{W}} + \boldsymbol{Z}_{1\mathrm{ow}}^{\mathrm{T}})^{-1} \right)^{-1} + \boldsymbol{Z}_{\mathrm{L}} \end{cases} \tag{D4}$$

where $\boldsymbol{Z}_{\mathrm{low}}^{\mathrm{T}}$ represents the impedance of the step-up transformer of wind turbine.

Hence, the total impedance of the wind farm is shown below.

$$\boldsymbol{Z}_{\mathrm{dq}}^{\mathrm{WF}} = \left(\left(\boldsymbol{Z}_{\mathrm{W\_4}}^{1}\right)^{-1} + \cdots + \left(\boldsymbol{Z}_{\mathrm{W\_4}}^{5}\right)^{-1} + \boldsymbol{Z}_{\mathrm{F3}} + \boldsymbol{Z}_{\mathrm{F5}} + \boldsymbol{Z}_{\mathrm{F7}} \right)^{-1} + \boldsymbol{Z}_{\mathrm{high}}^{\mathrm{T}} \tag{D5}$$

where the $\boldsymbol{Z}_{\mathrm{high}}^{\mathrm{T}}$ represents the impedance of the step-up transformer of wind farm. $\boldsymbol{Z}_{\mathrm{F3}}, \boldsymbol{Z}_{\mathrm{F5}}, \boldsymbol{Z}_{\mathrm{F7}}$ represents the impedance of the 3rd order, 5th order and 7th order filter branches.

The *d-q* impedance can be transformed to the modified sequence domain using (D5).

$$\boldsymbol{Z}_{\mathrm{Mpn}}^{\mathrm{WF}}(s) = \boldsymbol{A}_Z \boldsymbol{Z}_{\mathrm{dq}}^{\mathrm{WF}} \boldsymbol{A}_Z^{-1} \tag{D6}$$

$$\boldsymbol{A}_Z = \frac{1}{\sqrt{2}} \begin{bmatrix} 1 & j \\ 1 & -j \end{bmatrix}, \quad \boldsymbol{A}_Z^{-1} = \frac{1}{\sqrt{2}} \begin{bmatrix} 1 & 1 \\ -j & j \end{bmatrix} \tag{D7}$$

The 2 × 2 positive-sequence impedance of the wind farm is like

$$\boldsymbol{Z}_{\mathrm{P}}^{\mathrm{WF}}(s) = \boldsymbol{Z}_{\mathrm{Mpn}}^{\mathrm{WF}}(s) \tag{D8}$$

The 2 × 2 negative-sequence impedance of the wind farm is like

$$\boldsymbol{Z}_{\mathrm{N}}^{\mathrm{WF}}(s) = \boldsymbol{Z}_{\mathrm{Mpn}}^{\mathrm{WF}}(s + 2j\omega_1) \tag{D9}$$

E. SYMBOL DEFINITION

Equations are shown at the pages 14–17.

$$A(t) = \begin{bmatrix}
-\frac{R}{L} & 0 & 0 & -\frac{n_{\mathrm{ua}}^{\mathrm{s}}}{2L} & 0 & 0 & -\frac{n_{\mathrm{la}}^{\mathrm{s}}}{2L} & 0 & 0 & A[1,10] & A[1,11] & A[1,12] & A[1,13] & 0 & 0 & A[1,16] & 0 & 0 \\
0 & -\frac{R}{L} & 0 & 0 & -\frac{n_{\mathrm{ub}}^{\mathrm{s}}}{2L} & 0 & 0 & -\frac{n_{\mathrm{lb}}^{\mathrm{s}}}{2L} & 0 & A[2,10] & A[2,11] & A[2,12] & 0 & A[2,14] & 0 & 0 & A[2,17] & 0 \\
0 & 0 & -\frac{R}{L} & 0 & 0 & -\frac{n_{\mathrm{uc}}^{\mathrm{s}}}{2L} & 0 & 0 & -\frac{n_{\mathrm{lc}}^{\mathrm{s}}}{2L} & A[3,10] & A[3,11] & A[3,12] & 0 & 0 & A[3,15] & 0 & 0 & A[3,18] \\
\frac{n_{\mathrm{ua}}^{\mathrm{s}}}{C_{\mathrm{arm}}} & 0 & 0 & 0 & 0 & 0 & 0 & 0 & 0 & A[4,10] & A[4,11] & A[4,12] & A[4,13] & 0 & 0 & A[4,16] & 0 & 0 \\
0 & \frac{n_{\mathrm{ub}}^{\mathrm{s}}}{C_{\mathrm{arm}}} & 0 & 0 & 0 & 0 & 0 & 0 & 0 & A[5,10] & A[5,11] & A[5,12] & 0 & A[5,14] & 0 & 0 & A[5,17] & 0 \\
0 & 0 & \frac{n_{\mathrm{uc}}^{\mathrm{s}}}{C_{\mathrm{arm}}} & 0 & 0 & 0 & 0 & 0 & 0 & A[6,10] & A[6,11] & A[6,12] & 0 & 0 & A[6,15] & 0 & 0 & A[6,18] \\
\frac{n_{\mathrm{la}}^{\mathrm{s}}}{C_{\mathrm{arm}}} & 0 & 0 & 0 & 0 & 0 & 0 & 0 & 0 & A[7,10] & A[7,11] & A[7,12] & A[7,13] & 0 & 0 & A[7,16] & 0 & 0 \\
0 & \frac{n_{\mathrm{lb}}^{\mathrm{s}}}{C_{\mathrm{arm}}} & 0 & 0 & 0 & 0 & 0 & 0 & 0 & A[8,10] & A[8,11] & A[8,12] & 0 & A[8,14] & 0 & 0 & A[8,17] & 0 \\
0 & 0 & \frac{n_{\mathrm{lc}}^{\mathrm{s}}}{C_{\mathrm{arm}}} & 0 & 0 & 0 & 0 & 0 & 0 & A[9,10] & A[9,11] & A[9,12] & 0 & 0 & A[9,15] & 0 & 0 & A[9,18] \\
0 & 0 & 0 & \frac{n_{\mathrm{ua}}^{\mathrm{s}}}{L} & 0 & 0 & 0 & 0 & 0 & A[10,10] & A[10,11] & A[10,12] & A[10,13] & 0 & 0 & A[10,16] & 0 & 0 \\
0 & 0 & 0 & 0 & \frac{n_{\mathrm{ub}}^{\mathrm{s}}}{L} & 0 & 0 & 0 & 0 & A[11,10] & A[11,11] & A[11,12] & 0 & A[11,14] & 0 & 0 & A[11,17] & 0 \\
0 & 0 & 0 & 0 & 0 & \frac{n_{\mathrm{uc}}^{\mathrm{s}}}{L} & 0 & 0 & 0 & A[12,10] & A[12,11] & A[12,12] & 0 & 0 & A[12,15] & 0 & 0 & A[12,18] \\
0 & 0 & 0 & 0 & 0 & 0 & 0 & 0 & 0 & T_1 & 0 & 0 & 0 & -\frac{2\pi \cdot f_0}{\sqrt{3}} & \frac{2\pi \cdot f_0}{\sqrt{3}} & K_{\mathrm{iv}} & 0 & 0 \\
0 & 0 & 0 & 0 & 0 & 0 & 0 & 0 & 0 & 0 & T_1 & 0 & \frac{2\pi \cdot f_0}{\sqrt{3}} & 0 & -\frac{2\pi \cdot f_0}{\sqrt{3}} & 0 & K_{\mathrm{iv}} & 0 \\
0 & 0 & 0 & 0 & 0 & 0 & 0 & 0 & 0 & 0 & 0 & T_1 & 0 & -\frac{2\pi \cdot f_0}{\sqrt{3}} & \frac{2\pi \cdot f_0}{\sqrt{3}} & 0 & 0 & K_{\mathrm{iv}} \\
0 & 0 & 0 & 0 & 0 & 0 & 0 & 0 & 0 & -Z_L & 0 & 0 & 0 & 0 & 0 & -\frac{2\pi \cdot f_0}{\sqrt{3}} & \frac{2\pi \cdot f_0}{\sqrt{3}} \\
0 & 0 & 0 & 0 & 0 & 0 & 0 & 0 & 0 & 0 & -Z_L & 0 & 0 & 0 & 0 & \frac{2\pi \cdot f_0}{\sqrt{3}} & 0 & -\frac{2\pi \cdot f_0}{\sqrt{3}} \\
0 & 0 & 0 & 0 & 0 & 0 & 0 & 0 & 0 & 0 & 0 & -Z_L & 0 & 0 & 0 & 0 & -\frac{2\pi \cdot f_0}{\sqrt{3}} & \frac{2\pi \cdot f_0}{\sqrt{3}}
\end{bmatrix}$$

$$A[1,10]=\frac{K_{\mathrm{pi}}\left(-v^{\mathrm{s}}_{\mathrm{cua}}+v^{\mathrm{s}}_{\mathrm{cla}}\right)}{2V_{\mathrm{dc}}L}\quad A[3,10]=\frac{\sqrt{3}\,K_{\mathrm{id}}\left(-v^{\mathrm{s}}_{\mathrm{cuc}}+v^{\mathrm{s}}_{\mathrm{clc}}\right)}{6V_{\mathrm{dc}}L}\quad A[5,10]=-\frac{K_{\mathrm{id}}\left(i^{\mathrm{s}}_{\mathrm{cb}}+i^{\mathrm{s}}_{\mathrm{gb}}/2\right)}{\sqrt{3}\,V_{\mathrm{dc}}C_{\mathrm{arm}}}$$

$$A[7,10]=\frac{K_{\mathrm{pi}}\left(-i^{\mathrm{s}}_{\mathrm{ca}}+i^{\mathrm{s}}_{\mathrm{ga}}/2\right)}{V_{\mathrm{dc}}C_{\mathrm{arm}}}-\frac{n^{\mathrm{s}}_{\mathrm{la}}}{2C_{\mathrm{arm}}}\quad A[9,10]=\frac{K_{\mathrm{id}}\left(-i^{\mathrm{s}}_{\mathrm{cc}}+i^{\mathrm{s}}_{\mathrm{gc}}/2\right)}{\sqrt{3}\,V_{\mathrm{dc}}C_{\mathrm{arm}}}$$

$$A[1,11]=\frac{\sqrt{3}\,K_{\mathrm{id}}\left(-v^{\mathrm{s}}_{\mathrm{cua}}+v^{\mathrm{s}}_{\mathrm{cla}}\right)}{6V_{\mathrm{dc}}L}\quad A[3,11]=\frac{\sqrt{3}\,K_{\mathrm{id}}\left(v^{\mathrm{s}}_{\mathrm{cuc}}-v^{\mathrm{s}}_{\mathrm{clc}}\right)}{6V_{\mathrm{dc}}L}\quad A[5,11]=\frac{K_{\mathrm{pi}}\left(i^{\mathrm{s}}_{\mathrm{cb}}+i^{\mathrm{s}}_{\mathrm{gb}}/2\right)}{V_{\mathrm{dc}}C_{\mathrm{arm}}}+\frac{n^{\mathrm{s}}_{\mathrm{ub}}}{2C_{\mathrm{arm}}}$$

$$A[7,11]=\frac{K_{\mathrm{id}}\left(-i^{\mathrm{s}}_{\mathrm{ca}}+i^{\mathrm{s}}_{\mathrm{ga}}/2\right)}{\sqrt{3}\,V_{\mathrm{dc}}C_{\mathrm{arm}}}\quad A[9,11]=\frac{K_{\mathrm{id}}\left(i^{\mathrm{s}}_{\mathrm{cc}}-i^{\mathrm{s}}_{\mathrm{gc}}/2\right)}{\sqrt{3}\,V_{\mathrm{dc}}C_{\mathrm{arm}}}$$

$$A[1,12]=\frac{\sqrt{3}\,K_{\mathrm{id}}\left(v^{\mathrm{s}}_{\mathrm{cua}}-v^{\mathrm{s}}_{\mathrm{cla}}\right)}{6V_{\mathrm{dc}}L}\quad A[3,12]=\frac{K_{\mathrm{pi}}\left(-v^{\mathrm{s}}_{\mathrm{cuc}}+v^{\mathrm{s}}_{\mathrm{clc}}\right)}{2V_{\mathrm{dc}}L}\quad A[5,12]=\frac{K_{\mathrm{id}}\left(i^{\mathrm{s}}_{\mathrm{cb}}+i^{\mathrm{s}}_{\mathrm{gb}}/2\right)}{\sqrt{3}\,V_{\mathrm{dc}}C_{\mathrm{arm}}}$$

$$A[7,12]=\frac{K_{\mathrm{id}}\left(i^{\mathrm{s}}_{\mathrm{ca}}-i^{\mathrm{s}}_{\mathrm{ga}}/2\right)}{\sqrt{3}\,V_{\mathrm{dc}}C_{\mathrm{arm}}}\quad A[9,12]=\frac{K_{\mathrm{pi}}\left(-i^{\mathrm{s}}_{\mathrm{cc}}+i^{\mathrm{s}}_{\mathrm{gc}}/2\right)}{V_{\mathrm{dc}}C_{\mathrm{arm}}}-\frac{n^{\mathrm{s}}_{\mathrm{lc}}}{2C_{\mathrm{arm}}}$$

$$A[1,13]=\frac{K_{\mathrm{ii}}\left(v^{\mathrm{s}}_{\mathrm{cua}}-v^{\mathrm{s}}_{\mathrm{cla}}\right)}{2V_{\mathrm{dc}}L}\quad A[3,15]=\frac{K_{\mathrm{ii}}\left(v^{\mathrm{s}}_{\mathrm{cuc}}-v^{\mathrm{s}}_{\mathrm{clc}}\right)}{2V_{\mathrm{dc}}L}\quad A[5,14]=-\frac{K_{\mathrm{ii}}\left(i^{\mathrm{s}}_{\mathrm{cb}}+i^{\mathrm{s}}_{\mathrm{gb}}/2\right)}{V_{\mathrm{dc}}C_{\mathrm{arm}}}$$

$$A[7,13]=\frac{K_{\mathrm{ii}}\left(i^{\mathrm{s}}_{\mathrm{ca}}-i^{\mathrm{s}}_{\mathrm{ga}}/2\right)}{V_{\mathrm{dc}}C_{\mathrm{arm}}}\quad A[9,15]=\frac{K_{\mathrm{ii}}\left(i^{\mathrm{s}}_{\mathrm{cc}}-i^{\mathrm{s}}_{\mathrm{gc}}/2\right)}{V_{\mathrm{dc}}C_{\mathrm{arm}}}$$

$$A[1,16]=\frac{K_{\mathrm{pi}}K_{\mathrm{iv}}\left(v^{\mathrm{s}}_{\mathrm{cua}}-v^{\mathrm{s}}_{\mathrm{cla}}\right)}{2V_{\mathrm{dc}}L}\quad A[3,18]=\frac{K_{\mathrm{pi}}K_{\mathrm{iv}}\left(v^{\mathrm{s}}_{\mathrm{cuc}}-v^{\mathrm{s}}_{\mathrm{clc}}\right)}{2V_{\mathrm{dc}}L}\quad A[5,17]=\frac{K_{\mathrm{pi}}K_{\mathrm{iv}}\left(-i^{\mathrm{s}}_{\mathrm{cb}}-i^{\mathrm{s}}_{\mathrm{gb}}/2\right)}{V_{\mathrm{dc}}C_{\mathrm{arm}}}$$

$$A[7,16]=\frac{K_{\mathrm{pi}}K_{\mathrm{iv}}\left(i^{\mathrm{s}}_{\mathrm{ca}}-i^{\mathrm{s}}_{\mathrm{ga}}/2\right)}{V_{\mathrm{dc}}C_{\mathrm{arm}}}\quad A[9,18]=\frac{K_{\mathrm{pi}}K_{\mathrm{iv}}\left(i^{\mathrm{s}}_{\mathrm{cc}}-i^{\mathrm{s}}_{\mathrm{gc}}/2\right)}{V_{\mathrm{dc}}C_{\mathrm{arm}}}$$

$$A[2,10]=\frac{\sqrt{3}\,K_{\mathrm{id}}\left(v^{\mathrm{s}}_{\mathrm{cub}}-v^{\mathrm{s}}_{\mathrm{clb}}\right)}{6V_{\mathrm{dc}}L}\quad A[4,10]=\frac{K_{\mathrm{pi}}\left(i^{\mathrm{s}}_{\mathrm{ca}}+i^{\mathrm{s}}_{\mathrm{ga}}/2\right)}{V_{\mathrm{dc}}C_{\mathrm{arm}}}+\frac{n^{\mathrm{s}}_{\mathrm{ua}}}{2C_{\mathrm{arm}}}\quad A[6,10]=\frac{K_{\mathrm{id}}\left(i^{\mathrm{s}}_{\mathrm{cc}}+i^{\mathrm{s}}_{\mathrm{gc}}/2\right)}{\sqrt{3}\,V_{\mathrm{dc}}C_{\mathrm{arm}}}$$

$$A[8,10]=\frac{K_{\mathrm{id}}\left(i^{\mathrm{s}}_{\mathrm{cb}}-i^{\mathrm{s}}_{\mathrm{gb}}/2\right)}{\sqrt{3}\,V_{\mathrm{dc}}C_{\mathrm{arm}}}\quad A[10,10]=\frac{K_{\mathrm{pi}}\left(-v^{\mathrm{s}}_{\mathrm{cua}}-v^{\mathrm{s}}_{\mathrm{cla}}\right)}{V_{\mathrm{dc}}L}-\frac{R}{L}$$

$$A[2,11]=\frac{K_{\mathrm{pi}}\left(-v^{\mathrm{s}}_{\mathrm{cub}}+v^{\mathrm{s}}_{\mathrm{clb}}\right)}{2V_{\mathrm{dc}}L}\quad A[4,11]=\frac{K_{\mathrm{id}}\left(i^{\mathrm{s}}_{\mathrm{ca}}+i^{\mathrm{s}}_{\mathrm{ga}}/2\right)}{\sqrt{3}\,V_{\mathrm{dc}}C_{\mathrm{arm}}}\quad A[6,11]=-\frac{K_{\mathrm{id}}\left(i^{\mathrm{s}}_{\mathrm{cc}}+i^{\mathrm{s}}_{\mathrm{gc}}/2\right)}{\sqrt{3}\,V_{\mathrm{dc}}C_{\mathrm{arm}}}$$

$$A[8,11]=\frac{K_{\mathrm{pi}}\left(-i^{\mathrm{s}}_{\mathrm{cb}}+i^{\mathrm{s}}_{\mathrm{gb}}/2\right)}{V_{\mathrm{dc}}C_{\mathrm{arm}}}-\frac{n^{\mathrm{s}}_{\mathrm{lb}}}{2C_{\mathrm{arm}}}\quad A[10,11]=\frac{K_{\mathrm{id}}\left(-v^{\mathrm{s}}_{\mathrm{cua}}-v^{\mathrm{s}}_{\mathrm{cla}}\right)}{\sqrt{3}\,V_{\mathrm{dc}}L}$$

$$A[2,12]=\frac{\sqrt{3}\,K_{\mathrm{id}}\left(-v^{\mathrm{s}}_{\mathrm{cub}}+v^{\mathrm{s}}_{\mathrm{clb}}\right)}{6V_{\mathrm{dc}}L}\quad A[4,12]=\frac{-K_{\mathrm{id}}\left(i^{\mathrm{s}}_{\mathrm{ca}}+i^{\mathrm{s}}_{\mathrm{ga}}/2\right)}{\sqrt{3}\,V_{\mathrm{dc}}C_{\mathrm{arm}}}\quad A[6,12]=\frac{K_{\mathrm{pi}}\left(i^{\mathrm{s}}_{\mathrm{cc}}+i^{\mathrm{s}}_{\mathrm{gc}}/2\right)}{V_{\mathrm{dc}}C_{\mathrm{arm}}}+\frac{n^{\mathrm{s}}_{\mathrm{uc}}}{2C_{\mathrm{arm}}}$$

$$A[8,12]=\frac{K_{\mathrm{id}}\left(-i^{\mathrm{s}}_{\mathrm{cb}}+i^{\mathrm{s}}_{\mathrm{gb}}/2\right)}{\sqrt{3}\,V_{\mathrm{dc}}C_{\mathrm{arm}}}\quad A[10,12]=\frac{K_{\mathrm{id}}\left(v^{\mathrm{s}}_{\mathrm{cua}}+v^{\mathrm{s}}_{\mathrm{cla}}\right)}{\sqrt{3}\,V_{\mathrm{dc}}L}$$

$$A[2,14]=\frac{K_{\mathrm{ii}}\left(v^{\mathrm{s}}_{\mathrm{cub}}-v^{\mathrm{s}}_{\mathrm{clb}}\right)}{2V_{\mathrm{dc}}L}\quad A[4,13]=-\frac{K_{\mathrm{ii}}\left(i^{\mathrm{s}}_{\mathrm{ca}}+i^{\mathrm{s}}_{\mathrm{ga}}/2\right)}{V_{\mathrm{dc}}C_{\mathrm{arm}}}\quad A[6,15]=-\frac{K_{\mathrm{ii}}\left(i^{\mathrm{s}}_{\mathrm{cc}}+i^{\mathrm{s}}_{\mathrm{gc}}/2\right)}{V_{\mathrm{dc}}C_{\mathrm{arm}}}$$

$$A[8,14]=\frac{K_{\mathrm{ii}}\left(i^{\mathrm{s}}_{\mathrm{cb}}-i^{\mathrm{s}}_{\mathrm{gb}}/2\right)}{V_{\mathrm{dc}}C_{\mathrm{arm}}}\quad A[10,13]=\frac{K_{\mathrm{ii}}\left(v^{\mathrm{s}}_{\mathrm{cua}}+v^{\mathrm{s}}_{\mathrm{cla}}\right)}{V_{\mathrm{dc}}L}$$

$$A[2,17]=\frac{K_{\mathrm{pi}}K_{\mathrm{iv}}\left(v^{\mathrm{s}}_{\mathrm{cub}}-v^{\mathrm{s}}_{\mathrm{clb}}\right)}{2V_{\mathrm{dc}}L}\quad A[4,16]=\frac{K_{\mathrm{pi}}K_{\mathrm{iv}}\left(-i^{\mathrm{s}}_{\mathrm{ca}}-i^{\mathrm{s}}_{\mathrm{ga}}/2\right)}{V_{\mathrm{dc}}C_{\mathrm{arm}}}\quad A[6,18]=\frac{K_{\mathrm{pi}}K_{\mathrm{iv}}\left(-i^{\mathrm{s}}_{\mathrm{cc}}-i^{\mathrm{s}}_{\mathrm{gc}}/2\right)}{V_{\mathrm{dc}}C_{\mathrm{arm}}}$$

$$A[8,17]=\frac{K_{\mathrm{pi}}K_{\mathrm{iv}}\left(i^{\mathrm{s}}_{\mathrm{cb}}-i^{\mathrm{s}}_{\mathrm{gb}}/2\right)}{V_{\mathrm{dc}}C_{\mathrm{arm}}}\quad A[10,16]=\frac{K_{\mathrm{pi}}K_{\mathrm{iv}}\left(v^{\mathrm{s}}_{\mathrm{cua}}+v^{\mathrm{s}}_{\mathrm{cla}}\right)}{V_{\mathrm{dc}}L}$$

$$A[11,10]=\frac{K_{\mathrm{id}}\left(v^{\mathrm{s}}_{\mathrm{cub}}+v^{\mathrm{s}}_{\mathrm{clb}}\right)}{\sqrt{3}\,V_{\mathrm{dc}}L},\quad A[11,11]=\frac{K_{\mathrm{pi}}\left(-v^{\mathrm{s}}_{\mathrm{cub}}-v^{\mathrm{s}}_{\mathrm{clb}}\right)}{V_{\mathrm{dc}}L}-\frac{R}{L},\quad A[11,12]=-\frac{K_{\mathrm{id}}\left(v^{\mathrm{s}}_{\mathrm{cub}}+v^{\mathrm{s}}_{\mathrm{clb}}\right)}{\sqrt{3}\,V_{\mathrm{dc}}L},$$

$$A[11,14]=\frac{K_{\mathrm{ii}}\left(v^{\mathrm{s}}_{\mathrm{cub}}+v^{\mathrm{s}}_{\mathrm{clb}}\right)}{V_{\mathrm{dc}}L},\quad A[11,17]=\frac{K_{\mathrm{pi}}K_{\mathrm{iv}}\left(v^{\mathrm{s}}_{\mathrm{cub}}+v^{\mathrm{s}}_{\mathrm{clb}}\right)}{V_{\mathrm{dc}}L}$$

$$A[12,10]=-\frac{K_{\mathrm{id}}\left(v^{\mathrm{s}}_{\mathrm{cuc}}+v^{\mathrm{s}}_{\mathrm{clc}}\right)}{\sqrt{3}\,V_{\mathrm{dc}}L},\quad A[12,11]=\frac{K_{\mathrm{id}}\left(v^{\mathrm{s}}_{\mathrm{cuc}}+v^{\mathrm{s}}_{\mathrm{clc}}\right)}{\sqrt{3}\,V_{\mathrm{dc}}L},\quad A[12,12]=\frac{K_{\mathrm{pi}}\left(-v^{\mathrm{s}}_{\mathrm{cuc}}-v^{\mathrm{s}}_{\mathrm{clc}}\right)}{V_{\mathrm{dc}}L}-\frac{R}{L},$$

$$A[12,15]=\frac{K_{\mathrm{ii}}\left(v^{\mathrm{s}}_{\mathrm{cuc}}+v^{\mathrm{s}}_{\mathrm{clc}}\right)}{V_{\mathrm{dc}}L},\quad A[12,18]=\frac{K_{\mathrm{pi}}K_{\mathrm{iv}}\left(v^{\mathrm{s}}_{\mathrm{cuc}}+v^{\mathrm{s}}_{\mathrm{clc}}\right)}{V_{\mathrm{dc}}L}$$

REFERENCES

[1] A. Lesnicar and R. Marquardt, "An innovative modular multilevel converter topology suitable for a wide power range," in *Proc. IEEE Bologna Power Tech Conf.*, Bologna, Italy, vol. 3, 2003, p. 6.

[2] F. Deng, Q. Wang, D. Liu, Y. Wang, M. Cheng, and Z. Chen, "Reference submodule based capacitor monitoring strategy for modular multilevel converters," *IEEE Trans. Power Electron.*, vol. 34, no. 5, pp. 4711–4721, May 2019.

[3] C. Liu, F. Deng, Q. Heng, R. Zhu, M. Liserre, Z. Wang, and W. Chen, "Fault localization strategy for modular multilevel converters under submodule lower switch open-circuit fault," *IEEE Trans. Power Electron.*, vol. 35, no. 5, pp. 5190–5204, May 2020.

[4] L. P. Kunjumuhammed, B. C. Pal, C. Oates, and K. J. Dyke, "Electrical oscillations in wind farm systems: Analysis and insight based on detailed modeling," *IEEE Trans. Sustain. Energy*, vol. 7, no. 1, pp. 51–62, Jan. 2016.

[5] J. Lyu, X. Cai, and M. Molinas, "Frequency domain stability analysis of MMC-based HVdc for wind farm integration," *IEEE J. Emerg. Sel. Topics Power Electron.*, vol. 4, no. 1, pp. 141–151, Mar. 2016.

[6] J. Lyu, X. Cai, M. Amin, and M. Molinas, "Sub-synchronous oscillation mechanism and its suppression in MMC-based HVDC connected wind farms," *IET Gener., Transmiss. Distrib.*, vol. 12, no. 4, pp. 1021–1029, Feb. 2018.

[7] J. Lyu, M. Molinas, and X. Cai, "Stabilization control methods for enhancing the stability of wind farm integration via an MMC-based HVDC system," in *Proc. 11th IEEE Int. Conf. Compat., Power Electron. Power Eng. (CPE-POWERENG)*, Cádiz, Spain, 2017, pp. 324–329.

[8] J. Lyu, X. Cai, and M. Molinas, "Optimal design of controller parameters for improving the stability of MMC-HVDC for wind farm integration," *IEEE J. Emerg. Sel. Topics Power Electron.*, vol. 6, no. 1, pp. 40–53, Mar. 2018.

[9] M. Amin, A. Rygg, and M. Molinas, "Self-synchronization of wind farm in an MMC-based HVDC system: A stability investigation," *IEEE Trans. Energy Convers.*, vol. 32, no. 2, pp. 458–470, Jun. 2017.

[10] M. Zhu, Y. Xu, L. Chen, and H. Nian, "Impedance-based stability analysis of MMC-HVDC for offshore DFIG-based wind farms," in *Proc. 21st Int. Conf. Electr. Mach. Syst. (ICEMS)*, Jeju-do, South Korea, Oct. 2018, pp. 1139–1144.

[11] J. Sun and H. Liu, "Sequence impedance modeling of modular multilevel converters," *IEEE J. Emerg. Sel. Topics Power Electron.*, vol. 5, no. 4, pp. 1427–1443, Dec. 2017.

[12] J. Lyu, X. Zhang, X. Cai, and M. Molinas, "Harmonic state-space based small-signal impedance modeling of a modular multilevel converter with consideration of internal harmonic dynamics," *IEEE Trans. Power Electron.*, vol. 34, no. 3, pp. 2134–2148, Mar. 2019.

[13] H. Wu, X. Wang, and L. Kocewiak, "Impedance-based stability analysis of voltage-controlled MMCs feeding linear AC systems," *IEEE J. Emerg. Sel. Topics Power Electron.*, early access, doi: 10.1109/JESTPE.2019.2911654.

[14] C. Zhang, X. Cai, M. Molinas, and A. Rygg, "Frequency-domain modelling and stability analysis of a DFIG-based wind energy conversion system under non-compensated AC grids: Impedance modelling effects and consequences on stability," *IET Power Electron.*, vol. 12, no. 4, pp. 907–914, Apr. 2019.

[15] C. Zhang, X. Cai, M. Molinas, and A. Rygg, "On the impedance modeling and equivalence of AC/DC-side stability analysis of a grid-tied type-IV wind turbine system," *IEEE Trans. Energy Convers.*, vol. 34, no. 2, pp. 1000–1009, Jun. 2019.

[16] H. Zong, J. Lyu, X. Cai, C. Zhang, M. Molinas, and F. Rao, "Accurate aggregated modelling of wind farm systems in modified sequence domain for stability analysis," *Electric Power Syst. Res.*, vol. 175, Oct. 2019, Art. no. 105928.

[17] C. Zhang, M. Molinas, A. Rygg, and X. Cai, "Impedance-based analysis of interconnected power electronics systems: Impedance network modeling and comparative studies of stability criteria," *IEEE J. Emerg. Sel. Topics Power Electron.*, early access, doi: 10.1109/JESTPE.2019.2914560.

[18] H. Liu, X. Xie, C. Zhang, Y. Li, H. Liu, and Y. Hu, "Quantitative SSR analysis of series-compensated DFIG-based wind farms using aggregated RLC circuit model," *IEEE Trans. Power Syst.*, vol. 32, no. 1, pp. 474–483, Jan. 2017.

[19] G. Bergna, J. A. Suul, and S. D'Arco, "State-space modelling of modular multilevel converters for constant variables in steady-state," in *Proc. IEEE 17th Workshop Control Modeling Power Electron. (COMPEL)*, Trondheim, Norway, Jun. 2016, pp. 1–9.

[20] G. C. Paap, "Symmetrical components in the time domain and their application to power network calculations," *IEEE Trans. Power Syst.*, vol. 15, no. 2, pp. 522–528, May 2000.

[21] B. Wen, D. Boroyevich, R. Burgos, P. Mattavelli, and Z. Shen, "Analysis of D-Q small-signal impedance of grid-tied inverters," *IEEE Trans. Power Electron.*, vol. 31, no. 1, pp. 675–687, Jan. 2016.

[22] A. Rygg, M. Molinas, C. Zhang, and X. Cai, "A modified sequence-domain impedance definition and its equivalence to the dq-domain impedance definition for the stability analysis of AC power electronic systems," *IEEE J. Emerg. Sel. Topics Power Electron.*, vol. 4, no. 4, pp. 1383–1396, Dec. 2016.

[23] X. Wang, L. Harnefors, and F. Blaabjerg, "Unified impedance model of grid-connected voltage-source converters," *IEEE Trans. Power Electron.*, vol. 33, no. 2, pp. 1775–1787, Feb. 2018.

[24] M. Cespedes and J. Sun, "Impedance modeling and analysis of grid-connected voltage-source converters," *IEEE Trans. Power Electron.*, vol. 29, no. 3, pp. 1254–1261, Mar. 2014.

[25] H. Nian, L. Chen, Y. Xu, H. Huang, and J. Ma, "Sequences domain impedance modeling of three-phase grid-connected converter using harmonic transfer matrices," *IEEE Trans. Energy Convers.*, vol. 33, no. 2, pp. 627–638, Jun. 2018.

[26] C. Zhang, M. Molinas, A. Rygg, J. Lyu, and X. Cai, "Harmonic transfer-function-based impedance modeling of a three-phase VSC for asymmetric AC grid stability analysis," *IEEE Trans. Power Electron.*, early access, doi: 10.1109/TPEL.2019.2909576.

[27] C. Zhang, X. Cai, A. Rygg, and M. Molinas, "Sequence domain SISO equivalent models of a grid-tied voltage source converter system for small-signal stability analysis," *IEEE Trans. Energy Convers.*, vol. 33, no. 2, pp. 741–749, Jun. 2018.

[28] F. Liu, J. Liu, H. Zhang, and D. Xue, "Stability issues of $Z+Z$ type cascade system in hybrid energy storage system (HESS)," *IEEE Trans. Power Electron.*, vol. 29, no. 11, pp. 5846–5859, Nov. 2014.

HAOXIANG ZONG (Student Member, IEEE) received the B.Eng. degree in electrical engineering from Tianjin University, Tianjin, China, in 2017. He is currently pursuing the Ph.D. degree in electrical engineering with Shanghai Jiao Tong University, Shanghai, China. He was a Ph.D. Visiting Scholar at the Department of Engineering Cybernetics, Norwegian University of Science and Technology, Trondheim, Norway, in 2019. His current research interests are modeling and stability analysis of wind farm systems, where the aim is to establish the accurate model of the large-scale wind farm and study stability mechanisms of the wind farm with MMCs as the grid interface.

CHEN ZHANG received the B.Eng. degree from the China University of Mining and Technology, China, and the Ph.D. degree from Shanghai Jiao Tong University, China, in 2011 and 2018, respectively. He was a Ph.D. Visiting Scholar at the Department of Engineering Cybernetics, Norwegian University of Science and Technology (NTNU), Norway, in 2015, where he is currently a Postdoctoral Research Fellow. His research interests are modeling and stability analysis of VSC-based energy conversion systems, where the aim is to reveal the fundamental dynamics and stability mechanisms of renewable energies with VSCs as the grid interface.

JING LYU (Member, IEEE) received the B.Eng. degree in electrical engineering and automation from the China University of Mining and Technology, Jiangsu, China, in 2009, and the M.Eng. and Ph.D. degrees from Shanghai Jiao Tong University, Shanghai, China, in 2011 and 2016, respectively, both in electrical engineering.

He was a Postdoctoral Research Fellow at the Department of Engineering Cybernetics, Norwegian University of Science and Technology, Trondheim, Norway, from 2016 to 2017. He is currently a Tenure-Track Assistant Professor with the Department of Electrical Engineering, Shanghai Jiao Tong University. His main research interests include dynamic stability of MMC-based HVDC connected wind farms/PV plants, modeling and control of modular multilevel converter, wind power converters, and impedance modeling.

XU CAI received the B.Eng. degree in electrical engineering from Southeast University, Nanjing, China, in 1983, and the M.Eng. and Ph.D. degrees from the China University of Mining and Technology, Jiangsu, China, in 1988 and 2000, respectively, both in electrical engineering.

He was with the Department of Electrical Engineering, China University of Mining and Technology, as an Associate Professor, from 1989 to 2001. He was the Vice Director of the State Energy Smart Grid Research and Development Center, Shanghai, China, from 2010 to 2013. He has been with Shanghai Jiao Tong University, Shanghai, as a Professor, since 2002, where he has also been the Director of the Wind Power Research Center, since 2008. His current research interests include power electronics and renewable energy exploitation and utilization, including wind power converters, wind turbine control systems, large power battery storage systems, clustering of wind farms and its control systems, and grid integration.

MARTA MOLINAS (Member, IEEE) received the Diploma degree in electromechanical engineering from the National University of Asuncion, Asuncion, Paraguay, in 1992, the M.Eng. degree from Ryukyu University, Japan, in 1997, and the D.Eng. degree from the Tokyo Institute of Technology, Tokyo, Japan, in 2000. She was a Guest Researcher at the University of Padova, Padova, Italy, in 1998. From 2004 to 2007, she was a Postdoctoral Researcher at the Norwegian University of Science and Technology (NTNU), where she has been a Professor with the Department of Electric Power Engineering, from 2008 to 2014. She is currently a Professor with the Department of Engineering Cybernetics, NTNU. Her research interests include the stability of power electronics systems, harmonics, instantaneous frequency, and non-stationary signals from the human and the machine. She has been an AdCom Member of the IEEE Power Electronics Society, from 2009 to 2011. She is an Associate Editor of the IEEE JOURNAL OF EMERGING AND SELECTED TOPICS IN POWER ELECTRONICS (JESTPE), the IEEE POWER ELECTRONICS SOCIETY (PELS), and an Editor of the IEEE TRANSACTIONS ON ENERGY CONVERSION.

FANGQUAN RAO received the degree in electrical engineering from the Harbin Institute of Technology, Harbin, China, in 1958.

From 1958 to 1966, he was an Electrical Engineer at Harbin Electrical Machinery Works. From 1966 to 1999, he was with the Dongfang Electrical Machinery Company Ltd., Deyang, China. From 1983 to 1999, he was the Chief Engineer and also the Deputy Director of this company, where he took part in several significant hydro-power projects of China such as designing generators for power station Longyangxia (320 MW), and organized research on the 300-MW turbo generator and the hydro-generator with evaporation cooling system, which both won the Second Prize of the Chinese National Science and Technology Promotion. In 1999, he joined Shanghai Jiao Tong University, Shanghai, China, where he is currently a Professor with the Electrical Engineering Department. His research interests include the control of large electrical generators and special electrical machines.

Dr. Rao became a member of the Chinese Academy of Engineering, in 1995. He received the First Prize of the Chinese National Science and Technology Promotion from the Chinese Government and the Outstanding Prize of the Science and Technology Promotion of Sichuan Province.